



1 **Spatial and temporal evolution of future atmospheric**
2 **reactive nitrogen deposition in China under different climate**
3 **change mitigation strategies**

4 Mingrui Ma¹, Jiachen Cao^{2,3}, Dan Tong⁴, Bo Zheng⁵, Yu Zhao^{1,2*}

5

6 1. State Key Laboratory of Pollution Control and Resource Reuse and School of
7 Environment, Nanjing University, 163 Xianlin Rd., Nanjing, Jiangsu 210023, China.

8 2. Jiangsu Collaborative Innovation Center of Atmospheric Environment and
9 Equipment Technology (CICAEET), Nanjing University of Information Science and
10 Technology, Jiangsu 210044, China.

11 3. School of Environmental Science and Engineering, Nanjing University of
12 Information Science and Technology, Nanjing 210044, China.

13 4. Ministry of Education Key Laboratory for Earth System Modelling, Department of
14 Earth System Science, Tsinghua University, Beijing 100084, China

15 5. Institute of Environment and Ecology, Tsinghua Shenzhen International Graduate
16 School, Tsinghua University, Shenzhen 518055, China.

17

18

19 *Corresponding author: Yu Zhao

20 Phone: 86-25-89680650; email: yuzhao@nju.edu.cn

21



22 **Abstract**

23 Atmospheric reactive nitrogen (Nr) deposition plays a crucial role in linking air
24 pollution to ecosystem risks. Previous modeling studies have indicated that climate
25 change and pollution controls jointly result in significant changes in Nr deposition in
26 China. However, it remains unclear how future emission reductions will influence Nr
27 deposition under different climate pathways. Here, we investigated the spatiotemporal
28 evolution and driving factors of future Nr deposition under various national clean air
29 and climate policies. We applied WRF-CMAQ and assessed the historical (2010s,
30 2010-2014) pattern and future changes of Nr deposition till the 2060s (2060-2064) in
31 China, by combining two SSP-RCP global climate pathways and three national
32 emission control scenarios. The results show that the implementation of clean air and
33 carbon neutrality policies would greatly reduce oxidized nitrogen (OXN) deposition,
34 mitigate the adverse perturbations of climate change, and reduce the outflow from
35 Eastern China (EC) to the West Pacific. In North China (NC), the weakened
36 atmospheric oxidation capacity (AOC) would elevate the response of OXN deposition
37 to a 20% abatement of emissions (expressed as the ratio of percentage change of
38 deposition to emissions) from 82.6% in the 2010s to nearly 100% in the 2060s. In
39 contrast, the response of RDN deposition to NH₃ emissions would decline, likely
40 attributable to a more NH₃-rich condition. The outcomes of this work broaden scientific
41 understanding on how anthropogenic actions of air quality improvement and carbon
42 emission reduction would reshape the future Nr deposition and support effective
43 policymaking to reduce associated ecological damages.

44 **Keywords:** Nr deposition, SSP-RCP, climate change, outflow pollution, emission
45 abatement

47 **1. Introduction**

48 With vigorous development of industrial and agricultural activities worldwide



49 since the industrial revolution, the emissions of reactive nitrogen (Nr, including
50 oxidized and reduced nitrogen species, OXN and RDN, respectively) have increased
51 explosively (Kanakidou et al., 2016), elevating the Nr levels in both atmosphere and
52 deposition. Enriched ambient Nr has led to a series of regional haze and ozone (O₃)
53 pollution issues through participation in atmospheric aerosol formation and
54 photochemical reactions (Chen et al., 2021). Furthermore, excessive atmospheric Nr
55 deposits onto land and water bodies through both dry and wet forms, directly hurting
56 the stability and productivity of the entire ecosystem (Flower et al., 2013). Substantial
57 Nr deposition can result in diverse adverse ecological effects, such as water
58 eutrophication (Zheng et al., 2020), soil acidification (Raza et al., 2020), and
59 biodiversity loss (Liu et al., 2017).

60 China has undergone rapid industrialization and urbanization, accompanied with
61 explosive growth in the consumption of fossil fuels and fertilizers over the past few
62 decades, triggering significant emissions of NO_x and NH₃ (Zhao et al. 2013; Kang et al.
63 2016). Enhanced Nr emissions made the country one of the hotspots receiving largest
64 Nr deposition worldwide (Liu et al., 2013; Vet et al., 2014). Observations of background
65 sites from the China Nationwide Nitrogen Deposition Monitoring Network (NNDMN)
66 during 2011-2018 revealed that the annual averaged Nr deposition fluxes reached 23.6
67 kg N ha⁻¹ yr⁻¹, vastly surpassing the monitoring results in the United States (8.1 kg N
68 ha⁻¹ yr⁻¹), Europe (8.7 kg N ha⁻¹ yr⁻¹) and Japan (11.0 kg N ha⁻¹ yr⁻¹) (Wen et al., 2020).
69 Employing atmospheric chemistry transport models (CTMs) or advanced statistical
70 models, a series of studies have indicated that Nr deposition fluxes has increased nearly
71 60% since 1980s, notably in eastern China (Gao et al., 2023, Yu et al. 2019, Zhao et al.,
72 2022, Zhou et al., 2023). Evidently, China is still struggling with serious Nr pollution.
73 The national air pollution control actions over the past decade have resulted in a fast
74 decline in emissions of acidic gaseous pollutants (mainly NO_x and SO₂) but relatively
75 stable NH₃ (Zheng et al., 2018). The imbalance in emission reductions for different
76 species has altered the composition of Nr deposition, e.g., a growth in the proportion of
77 RDN (Liu et al., 2020). More importantly, the increasingly strong capacity of



78 atmospheric oxidation, attributed primarily to the persistently high emissions of volatile
79 organic compounds (VOCs), has been weakening the response of OXN deposition to
80 NO_x emissions in eastern part of China and thus preventing effective reduction of Nr
81 deposition. One-unit abatement of NO_x emissions resulted in only less than 80% of
82 OXN deposition, emphasizing the crucial role of active O₃-VOCs-NO_x photochemistry
83 in modulating the Nr deposition (Liu et al., 2022).

84 Atmospheric Nr deposition are mainly influenced by rainfall, precursor emissions,
85 and long-distance transport (Ellis et al., 2013, Kim et al., 2012, Ma et al., 2023, Zhu et
86 al., 2022). The strengthening climate change and implementation of pollution controls
87 will greatly alter the regional meteorological conditions and air pollutant emissions,
88 resulting in substantial changes in magnitude and spatiotemporal pattern of Nr
89 deposition. The changing deposition will further exert multiple impacts on the
90 biodiversity, carbon sequestration and greenhouse emissions of various ecosystems,
91 and thus influence the climate and ecological environment profoundly (Zhu et al., 2020).
92 There are only a few studies addressing future Nr deposition in China. They employed
93 coupled climate-chemistry global models to conduct simulations under different
94 predefined greenhouse gas (GHG) emission scenarios. Future emissions were primarily
95 referencing the Intergovernmental Panel on Climate Change (IPCC) Representative
96 Concentration Pathways (RCPs) based on the radiative forcing in 2100 (van Vuuren et
97 al., 2011). A pioneering study by Galloway et al. (2004) predicted significant growth in
98 Nr deposition in East Asia, exceeding 50 kg N ha⁻¹ year⁻¹ based on the IPCC92a
99 emission scenario. The Atmospheric Chemistry and Climate Model Intercomparison
100 Project (ACCMIP) presented a multi-model global datasets of Nr deposition, covering
101 the period from 1850 to 2100 (Lamarque et al. 2013a). The Nr deposition in East Asia
102 was estimated to increase 27% and 39% in the 2030s under the RCP2.6 and RCP8.5
103 pathways, respectively (Lamarque et al. 2013b). More recently, Zhang et al. (2019) and
104 Sun et al. (2022) reported the possible future changes in OXN and RDN deposition,
105 respectively, based on ACCMIP datasets. The OXN deposition fluxes under both
106 RCP4.5 and RCP8.5 pathways were projected to increase in 2030s but decrease by the



107 end of the century, driven primarily by the Nr emission trends. The proportion of RDN
108 in total deposition in eastern China was projected to rise from 38% in 2000 to 56% in
109 2100 under RCP8.5 pathway, suggesting a transition in the dominant form from
110 oxidized to reduced.

111 Even previous studies made insightful predictions on the future evolution of Nr
112 deposition in China, they have insufficiently incorporated the potentially profound
113 emission reduction in the context of global climate change. In 2020, China announced
114 the plan to achieve carbon neutrality by 2060, and the effects of a wide range of sharp
115 emission reductions on future environment has become a major research focus (Dong
116 et al., 2021). Researchers have integrated national strategies of emission reduction to
117 assess future air pollution and associated health risks in China under various climate
118 change pathways (Cheng et al., 2021a, Cheng et al., 2023, Shi et al., 2021). For example,
119 the IPCC Sixth Assessment Report (AR6) introduced a scientifically combined set of
120 pathways known as Shared Socioeconomic Pathways (SSPs) and RCPs, denoted as
121 SSP-RCP (IPCC, 2021). New pathways integrate the impact of socioeconomic
122 development into the framework for the evolution of GHG levels, offering more reliable
123 projections of possible outcomes of climate change (Cook et al., 2020; O'Neill et al.,
124 2016, Xin et al., 2020). However, there is a noticeable gap in assessment of China's
125 atmospheric deposition under the SSP-RCP framework. The roles of future emission
126 and climate changes on deposition remain unclear across diverse climate pathways.
127 Moreover, stringent emission controls with diverse progresses for various species and
128 regions will change the atmospheric oxidizing capacity and regional transport of
129 pollution, and thereby alter the response of Nr deposition to emissions of their
130 precursors. Given the crucial role of atmospheric deposition in connecting air pollution
131 to ecosystem risks, it is essential to evaluate these anticipated changes for a
132 comprehensive understanding of the ecological and environmental impacts during the
133 long-term progress of continuous air quality improvement and global warming
134 prevention.

135 In this study, we applied an air quality model (WRF-CMAQ, see details in methods)



136 and assessed the future changes of Nr deposition in China, by combining the SSP-RCP
137 global climate change pathways and the national emission control scenarios. The
138 historical period was chosen as 2010-2014, representing the years with the highest Nr
139 emissions in China, and the future simulation period was determined as 2060-2064.
140 Firstly, we evaluated the model performance of meteorology and Nr deposition for the
141 historical period based on available ground observations. We then quantified the spatial
142 and temporal changes of future Nr deposition and identified the main driving factors
143 under two IPCC pathways, SSP2-4.5 and SSP5-8.5). The SSP5-8.5 pathway represents
144 high GHG emissions characterized by continued reliance on fossil fuels, often viewed
145 as a pessimistic outlook for future climate change. Conversely, the SSP2-4.5 pathway
146 envisions moderate GHG emissions, achieved through the consideration of
147 environmental policies and technological advancements. We further assessed the effects
148 of various emissions abatement scenarios on Nr deposition. Finally, we analyzed the
149 future response of deposition to emission perturbation under different scenarios. The
150 study enhances scientific understanding on the interactions between anthropogenic
151 activities and atmospheric chemistry along with a changing climate, and in turn
152 supports the development of effective environmental policies to alleviate the adverse
153 effects of Nr pollution on ecosystems and human health.

154 **2. Methodology and data**

155 **2.1 Model description and driving data**

156 The Community Multiscale Air Quality (CMAQ) model version 5.2 (available at
157 <https://epa.gov/cmaq/access-cmaq-source-code>) was adopted to conduct atmospheric
158 Nr deposition simulations over mainland China for both historical (2010-2014) and
159 future periods (2060-2064). To avoid the model errors associated with individual years,
160 full-year simulations were conducted for every year of the two five-year intervals, and
161 the five-year averages were used for further analyses. A series of simulation cases were
162 designed by combining individual climate pathways and national emission scenarios to



163 separate the roles of multiple factors on future deposition (see details in Section 2.2).
164 Developed by the United States Environmental Protection Agency (USEPA), CMAQ
165 has been demonstrated to possess extensive practicality and sophistication in simulating
166 regional air quality and acid deposition (Appel et al., 2017, Chang et al., 2020, Cheng
167 et al., 2021, Liu et al., 2010). A single domain covering mainland China (186×156 grid
168 cells) was adopted for the simulations with a horizontal resolution at 27×27 km per
169 grid (Figure S1). Lambert conformal conic projection was applied for the domain
170 centered at (102°E , 37°N) with two true latitudes, 40°N and 25°N . In the vertical
171 direction, 30 eta levels with the pressure of 50hPa at the top level were used. For
172 chemical configuration, the carbon bond 05 (CB05) gas-phase chemical scheme and
173 the AERO 6 aerosol scheme were adopted (Sarwar et al., 2008, Pye et al., 2017, Murphy
174 et al., 2017). The boundary condition of trace gases used in this study was background
175 concentration (default setup in CMAQ model). Simulation of each year included a one-
176 month spin-up time (i.e., 1st-31st December of the previous year) to reduce the impact
177 of the initial conditions on the simulations.

178 The Multi-resolution Emission Inventory for China version 1.3 developed by
179 Tsinghua University (MEICv1.3, available at
180 http://www.meicmodel.org/?page_id=560; Li et al., 2017; Zheng et al., 2018) provided
181 historical anthropogenic emission data within China in our simulations. Information on
182 future emissions were obtained from the Dynamic Projection model for Emissions in
183 China version 1.1 developed by Tsinghua University (DPECv1.1, available at
184 http://meicmodel.org.cn/?page_id=1917). DPEC links global climate mitigation
185 pathways to local clean air policies and fully incorporates China's strict air pollution
186 control progress since the implementation of the “Action Plan of Air Pollution
187 Prevention and Control” in 2013. It thus corrects the erroneous emission trends of China
188 in the Coupled Model Intercomparison Project (CMIP) scenarios (Cheng et al., 2021b;
189 Tong et al., 2020). Three emission scenarios, named as “Baseline”, “Current-goal”, and
190 “Neutral-goal”, were used in this work (see the simulation case design in Section 2.2).
191 The “Baseline” depicts a high-emission scenario in the absence of climate and pollution



192 control policies, equivalent to the SSP5-8.5 climate pathway. The “Current-goal”
193 scenario is a combination that takes into account SSP2-4.5 climate pathway along with
194 existing pollution control policies in China. The “Neutral-goal” scenario integrates
195 China's 2060 carbon neutrality goal with the most stringent pollution control policies.
196 Details of the scenarios were described in Cheng et al. (2021b).

197 Anthropogenic emissions outside of China were taken from the Asian
198 anthropogenic emission inventory, named MIX, developed by the Model Inter-
199 Comparison Study for Asia (MICS-Asia) project (available at
200 http://meicmodel.org.cn/?page_id=1770; Li et al., 2017). Biogenic emissions were
201 calculated by the Model Emissions of Gases and Aerosols from Nature developed under
202 the Monitoring Atmospheric Composition and Climate project version 2.1
203 (MEGANv2.1; Guenther et al., 2012). The initial horizontal resolutions of both
204 emission inventories were $0.25^\circ \times 0.25^\circ$, and they were interpolated into our simulation
205 domain with the resolution of 27 km.

206 The Weather Research and Forecasting (WRF) model version 3.9.1 (available at
207 https://www2.mmm.ucar.edu/wrf/users/wrf_files/wrfv3.9/updates-3.9.1.html) was
208 applied to provide meteorological fields for CMAQ. Developed and maintained
209 collaboratively by the National Center for Atmospheric Research (NCAR) and the
210 National Oceanic and Atmospheric Administration (NOAA), WRF model has been
211 recognized as a state-of-the-art regional weather model and widely utilized in short-
212 term weather forecasting and regional meteorological research (Huang et al., 2020,
213 Skamarock et al., 2008, Wang et al., 2021). For our historical meteorological simulation,
214 the fifth generation of European Centre for Medium-Range Weather Forecasts
215 (ECMWF) reanalysis dataset, ERA5 (available at
216 [https://cds.climate.copernicus.eu/cdsapp#!/dataset/reanalysis-era5-single-](https://cds.climate.copernicus.eu/cdsapp#!/dataset/reanalysis-era5-single-levels?tab=form)
217 [levels?tab=form](https://cds.climate.copernicus.eu/cdsapp#!/dataset/reanalysis-era5-single-levels?tab=form)) was adopted as the initial and boundary field (Hersbach et al., 2020).
218 The temporal and spatial resolution was 6 hours and $0.25^\circ \times 0.25^\circ$, respectively. For
219 simulation of future period, it is commonly practical to employ climate forecast results
220 from global climate models (GCMs) as the initial and boundary conditions. In this study,



221 a global bias-corrected multi-model (BCMM) climatological dataset with a horizontal
222 resolution of $1.25^{\circ} \times 1.25^{\circ}$ at 6-hour intervals (available at
223 <https://www.scidb.cn/en/detail?dataSetId=791587189614968832#p2>) was adopted to
224 drive WRF model for 2060-2064. The BCMM dataset was reconstructed from 18
225 GCMs of the CMIP6, with corrections for climatological mean and interannual variance
226 biases based on ERA5 data from 1979-2014, providing more reliable projections of
227 long-term non-linear trends of multiple climate variables compared with original
228 CMIP6 model outputs. Details of BCMM product were described at Xu et al. (2021).
229 We employed Pseudo Global Warming (PGW) method (Kawase et al., 2013, Liu et al.,
230 2021, Lauer et al., 2013, Taniguchi et al., 2020) for statistical downscaling. Specifically,
231 future driving fields were forced with the ERA5 data from reference period (2010-2014)
232 plus a climate perturbation (difference between the years 2060-2064 and 2010-2014)
233 calculated from BCMM results, as shown in Eq. (1) and Eq (2):

$$234 \quad WRF_{input2060-2064} = ERA5_{2010-2014} + \Delta BCMM_{ssp} \quad (1)$$

$$235 \quad \Delta BCMM_{ssp} = BCMM_{\overline{2060-2064}} - BCMM_{\overline{2010-2014}} \quad (2)$$

236 where $\Delta BCMM_{ssp}$ is the CMIP6 multimodel ensemble mean change signal for 2060-
237 2064 relative to 2010-2014 under the SSP2-4.5 or SSP5-8.5 pathway, $BCMM_{\overline{2060-2064}}$
238 and $BCMM_{\overline{2010-2014}}$ represent the 5-year meteorological averages of BCMM dataset
239 in the future and reference periods, respectively. Nine physical variables were perturbed
240 in this study including zonal wind, meridional wind, air temperature, sea surface
241 temperature, soil temperature, specific humidity, the surface pressure, sea-level
242 pressure and geopotential height. The bilinear interpolation was applied to interpolate
243 BCMM data to the ERA5 grid.

244 The land-use and land-cover (LULC) data were taken from global data of the U.S.
245 Geological Survey (USGS) (de Meij et al., 2014; Pineda et al., 2004). The physical
246 parameterization schemes used in all simulations are summarized in Table S1 in the
247 Supplement.

248 The dry deposition (DDEP) of each atmospheric chemical species (i) was
249 calculated as the product of surface concentration ($C^{surface}$) and dry deposition velocity



250 (V_d) at the lowest model layer, as shown in Eq. (3):

$$251 \quad DDEP_i = C_i^{surface} \times V_d \quad (3)$$

252 According to the classical resistance cascade model (Venkatram and Pleim, 1999;
253 Wesely, 2007), the parameters of V_d are calculated as Eq. (4):

$$254 \quad V_d = 1/(R_a + R_b + R_c) \quad (4)$$

255 where R_a is the aerodynamic resistance to the transfer from lowest layer to the
256 roughness height, calculated as a function of surface layer turbulence parameters
257 including friction velocity and the Monin-Obukhov length; R_b is the boundary layer
258 resistance to transfer between the roughness height and surface; R_c is the resistance to
259 surface uptake, which can be further divided into several series and parallel components,
260 representing the resistance to the lower vegetation canopy or ground.

261 The algorithm module for wet deposition (WDEP) is derived from the regional
262 acid deposition model (RADM; Chang et al., 1987) and depends on the precipitation
263 rate (P_r) and cloud water concentration (C_{cloud}) of specific chemical component:

$$264 \quad WDEP_i = P_r \cdot \bar{C}_i^{cloud} \quad (5)$$

265 The wet scavenging is considered in two pathways, depending upon whether the
266 pollutant participates in the cloud water chemistry and on the liquid water content.

267 Details on how CMAQ removes pollutants through wet deposition can be found in the
268 official CMAQ Science Documentation (available at

269 https://www.cmascenter.org/cmaq/science_documentation/pdf/ch11.pdf). In this study,

270 OXN included NO, NO₂, HNO₃, N₂O₅, HONO, and particulates as nitrate (NO₃⁻), and

271 RDN included NH₃ and particulates as ammonium (NH₄⁺).

272 2.2 Numerical simulation experiment design

273 To evaluate future changes in the spatiotemporal pattern of atmospheric Nr
274 deposition under different SSP-RCP climate pathways and emission control scenarios,
275 we performed parallel numerical simulation experiments with WRF-CMAQ, as
276 summarized in Table 1. Base simulated the real situation in historical period (2010-
277 2014). Case 1 and Case 2 were designed to predict the atmospheric Nr deposition in the



278 2060s, following SSP2-4.5 climate pathway with “Current-goal” emission scenario in
279 DPEC and SSP5-8.5 climate pathway with “Baseline” emission scenario, respectively.
280 Difference between Case 1 and Base and that between Case 2 and Base respectively
281 revealed the changing Nr deposition from 2010s to 2060s in SSP2-4.5 and SSP5-8.5.

282 Cases 3 and 4 applied future climate pathways (SSP2-4.5 and SSP5-8.5,
283 respectively) but historical emissions, and the difference between each of them and
284 Base revealed how climate change would influence Nr deposition under corresponding
285 climate pathway. Meanwhile, the effect of emission change on future Nr deposition was
286 examined by comparing Case 3 and Case 1 for “Current-goal” scenario in DPEC, and
287 by comparing Case 4 and Case 2 for “Baseline” scenario. Case 5 applied SSP2-4.5
288 climate pathway and “Neutral-goal” emission scenario in DPEC. Comparison between
289 Case 5 and Case 3 revealed the benefit of national emission controls under China’s
290 carbon neutrality policy on Nr deposition.

291 Cases 6-8 were designed based on Cases 1, 3, and 5, respectively. In these cases,
292 emissions in eastern China (EC) were set at the 2060s level, while those in western
293 China (WC) were maintained at the 2010s level. The aim was to explore the effect of
294 diverse emission control progresses for different regions on the future Nr deposition.
295 WC and EC were divided by longitude 110° east in this study, as shown in Figure S1.
296 In Cases 9-12, the emissions of all species were reduced by 20% from those in Cases 3,
297 1, 2, and 5, respectively, to explore the response of deposition to emission perturbation
298 at different atmospheric conditions caused by varying pollution control levels.

299 **2.3 Observations and model evaluation**

300 WRF-CMAQ model performance was evaluated against available observation of
301 meteorological variables and Nr deposition at monthly or annual level. Daily near-
302 surface observations of four meteorological parameters including temperature at the
303 height of 2 m (T2), relative humidity (RH), wind speed at the height of 10 m (WS10)
304 and accumulated precipitation (PREC) were derived from the National Meteorological
305 Data Center of China Meteorological Administration (CMA,



306 <http://data.cma.cn/data/detail/dataCode/A.0012.0001.html>). The 839 meteorological
307 surface stations, with continuous five-year observations from 2010 to 2014 were
308 selected, as shown in Figure 1. Meanwhile, the monthly observations of Nr deposition
309 fluxes were taken from the Nationwide Nitrogen Deposition Monitoring Network
310 (NNDMN; Xu et al., 2018; 2019). Following our previous study, we selected 28 sites
311 for dry deposition fluxes and 53 sites for wet deposition fluxes, for which at least two-
312 year continuous measurement data were available, to evaluate model performance.
313 Details of monitoring stations can be found in Ma et al. (2023). Statistical indicators
314 were calculated with Eq. (6-9), including normalized mean bias (NMB), normalized
315 mean error (NME) and the correlation coefficient (R) at temporal and spatial scales
316 (Baker et al., 2004; Ma et al., 2023):

$$317 \quad NMB = \frac{\sum_{i=1}^n (S_i - O_i)}{\sum_{i=1}^n O_i} \times 100\% \quad (6)$$

$$318 \quad NME = \frac{\sum_{i=1}^n |S_i - O_i|}{\sum_{i=1}^n O_i} \times 100\% \quad (7)$$

$$319 \quad R(temporal) = \frac{\sum_{i=1}^n (S_i - \bar{S})(O_i - \bar{O})}{\sqrt{\sum_{i=1}^n (S_i - \bar{S})^2 (O_i - \bar{O})^2}} \quad (8)$$

$$320 \quad R(spatial) = \frac{\sum_{j=1}^m (\bar{S}_j - \bar{S}_j)(\bar{O}_j - \bar{O}_j)}{\sqrt{\sum_{j=1}^m (\bar{S}_j - \bar{S}_j)^2 (\bar{O}_j - \bar{O}_j)^2}} \quad (9)$$

321 where S and O are the monthly meteorological variables or annual Nr deposition from
322 model simulation and observation, respectively; \bar{S} and \bar{O} are the monthly mean
323 meteorological variables or annual deposition from model simulation and observation,
324 respectively; i means the individual month or year and j means the individual site.

325 **3. Results and discussion**

326 **3.1 Evaluation of model performance**

327 We compared the simulated near-surface temperature, wind speed, relative
328 humidity and accumulated precipitation with observations at the monthly level, as
329 shown in Figure 1. The model reasonably reproduced the spatial pattern of near-surface
330 temperature with the spatial R reaching 0.95 (Figure 1a). Overestimation was found in
331 the southeast and northwest of the country while underestimation over the Tibetan



332 Plateau. At the national scale, T2 was generally underestimated with the NMB and
333 NME calculated at -7.76% and 12.75%, respectively. In addition, the temporal R
334 reached 0.99, indicating the simulation was in good agreement with observation at the
335 monthly level. Unlike T2, due to the modeling biases in the topographic effects and the
336 underestimation of urban land use in USGS (Carvalho et al., 2012; Liao et al., 2015),
337 WS10 was overestimated with NMB calculated at 33.13% at the national scale (Figure
338 1b). Such overestimation was also reported in other studies (Liu et al., 2020, Shen et
339 al., 2021, Zhu et al., 2022). RH is slightly underestimated with NMB and NME
340 calculated at -1.58% and 8.94%, respectively, while both spatial and temporal R were
341 greater than 0.8 (Figure 1c). PREC was generally underestimated, with NMB and NME
342 at -19.39% and 39.15%, respectively. A clear gradient from northwest to southeast
343 China was well captured, and the temporal and spatial R were 0.83 and 0.76,
344 respectively (Figure 1d).

345 The comparison between the simulated and observed annual Nr deposition
346 averaged over 2010-2014 at the site level are provided by form (dry and wet) and
347 species (OXN and RDN) in Table 2. Nr deposition was underestimated for all cases.
348 The NMB and NME for the dry deposition of OXN (DDEP_OXN) were calculated at
349 -9.07% and 24.76%, respectively, and the analogous numbers for RDN (DDEP_RDN)
350 were at -15.12% and 43.24%. The uncertainty in NH₃ emission inventories was
351 frequently recognized as an important factor contributing to the underestimation (Ma
352 et al., 2023, Chang et al., 2020, Shen et al., 2023). The limited development of intensive
353 livestock breeding and farming in China poses a considerable challenge in acquiring
354 sufficient activity data and accurate emission factors, leading to underestimation of
355 emissions with the “bottom-up” approach. Utilizing satellite constraints, Zhang et al.
356 (2018) estimated that the total NH₃ emissions in China may be underestimated by nearly
357 40%. Due to lack of direct observation, additionally, the dry deposition at NNDMN
358 sites was calculated by multiplying the observed surface concentrations with V_d
359 simulated from GEOS-Chem (Bey et al., 2001; Xu et al., 2019). Difference in the
360 parameterization schemes for calculating V_d of given trace gases or aerosols between



361 CTMs could also introduce modest uncertainty for assessment of OXN deposition (Wu
362 et al., 2018; Chang et al., 2020). Compared to dry deposition, wet deposition of OXN
363 and RDN (WDEP_OXN and WDEP_RDN) was simulated to be far lower than the
364 observations, with the NMBs calculated at -28.76% and -17.86%, respectively. Part of
365 the reason may be underestimation of precipitation (Figure 1d). More importantly, most
366 of wet deposition measured at NNDMN sites was actually “bulk deposition”, which
367 included both wet deposition and a small fraction of dry deposition (Xu et al., 2015).
368 Therefore, the bias from observation also contributed to the inconsistency.

369 Project of the Model Inter-Comparison Study for Asia (MICS-Asia) phase III
370 reported the performances of Nr deposition simulation with multiple models over China,
371 with the overall NMBs and NMEs ranged -47% – 67% and 48% – 82% for OXN, and
372 -70% – -29% and 44% – 72% for RDN, respectively (Ge et al., 2020). The model
373 performance in our study was comparable to previous studies. In addition, both spatial
374 and temporal R were greater than 0.6 for each deposition form and species. Overall, our
375 simulations reasonably reproduced the observed Nr deposition in both magnitude and
376 spatiotemporal patterns.

377 **3.2 Evolution of Nr deposition and the roles of climate and emission** 378 **changes**

379 Table 3 summarizes the simulated atmospheric Nr deposition over historical (Base)
380 and future periods under SSP2-4.5 (Case 1) and SSP5-8.5 pathways (Case 2). The
381 annual averaged Nr deposition for 2010-2014 was simulated at 14.7 kg N ha⁻¹ yr⁻¹ for
382 mainland China (Base). The contribution of RDN to total deposition reached 52%,
383 which was in good agreement with the multiple-model ensemble mean value in the
384 MICS-Asia phase III project (Ge et al., 2020). The ratio of wet deposition to total
385 deposition was 0.54 in our simulation, also close to other CTM and nationwide
386 observation results (Ge et al., 2020, Xu et al., 2015, Zhao et al., 2017).

387 Under the SSP2-4.5 pathway, total Nr deposition would decrease to 9.0 kg N ha⁻¹
388 yr⁻¹ during 2060-2064, primarily attributed to a sharp decline in OXN deposition (Case



389 1). Accompanied with an active energy transition and effective control of fossil fuel
390 consumption, the substantial reduction of anthropogenic NO_x emissions led to a 56%
391 decline in OXN deposition compared to the reference period. Meanwhile, RDN
392 deposition would be reduced by only 22%, resulting from a modest abatement of NH_3
393 emissions. Figure S2 in the supplement shows the changes of NO_x and NH_3 emissions
394 in 2060 relative to the historical period (2010-2014) in various scenarios, and Figure
395 S3 in the supplement provides the annual emissions by sector. Large emission changes
396 would occur mainly in the east of China. By 2060s, the national NO_x emissions would
397 decline 55% (-15.1 Mt) under the “Current-goal” emission scenario. Such reductions
398 would come mainly from power, industry and transportation sectors, driven by the
399 predicted transition of energy structure (Figures S3a-b). Due to less improvement in
400 agriculture management, the NH_3 emissions would decline much slower by 28% (-2.9
401 Mt). Under the SSP5-8.5 pathway, the global economy would maintain rapid growth
402 without sufficient considerations for climate change. A high dependence on fossil fuels
403 (especially coal) for energy consumption would result in a nationwide growth of annual
404 NO_x emissions by 24% (6.5 Mt) from 2010s to 2060s (“Baseline” scenario in DPEC,
405 Figure S2a), and thereby elevate the total Nr deposition to $15.4 \text{ kg N ha}^{-1} \text{ yr}^{-1}$ (Case 2).
406 The proportions of OXN and RDN in future Nr deposition were anticipated to vary
407 across different SSP-RCP pathways. Under the SSP2-4.5 pathway, RDN was predicted
408 to be the dominant species of Nr deposition in the 2060s, with a proportion to the total
409 estimated at 66%. Under the SSP5-8.5 pathway, the proportion of OXN to total
410 deposition was expected to expand from 48% in the 2010s to 55% in the 2060s.

411 In terms of spatial pattern, our simulations present clearly larger regional
412 difference in China compared to the global results of ACCMIP, owing to finer
413 simulation resolution and more detailed regional emission information. Figure 2
414 illustrates the spatial distribution of Nr deposition in historical period and the future
415 changes under different SSP-RCP pathways. For 2010-2014, a clear gradient from west
416 to east was found for all deposition forms and species (Figures 2a-d), driven mainly by
417 the spatial distributions of NH_3 and NO_x emissions. Dry deposition of OXN



418 (DDEP_OXN) appeared mainly in eastern China, especially in the Beijing-Tianjin-
419 Hebei (BTH), Yangtze River Delta (YRD) and Pearl River Delta (PRD) regions (see
420 Figure S1 for the locations of these regions), resulting mainly from the large NO_x
421 emissions caused by active industrialization and urbanization. Hotspots of RDN dry
422 deposition (DDEP_RDN) appeared mainly in the North China Plain and the Sichuan
423 Basin (SCB) with intensive agricultural activities. Further influenced by precipitation
424 patterns, the southern areas experienced greater wet deposition compared to the north,
425 consistent with previous studies (Han et al., 2017; Zhao et al., 2017). Influenced jointly
426 by the substantial rainfall and local Nr emissions, in particular, SCB was of the largest
427 wet deposition for both OXN and RDN (WDEP_OXN and WDEP_RDN).

428 The future OXN deposition would exhibit contrasting trends between the SSP2-
429 4.5 and SSP5-8.5 pathways. Compared to historical periods, both dry and wet forms
430 were predicted to decrease in the 2060s under the SSP2-4.5 pathway, with national
431 average reductions of 2.2 kg N ha⁻¹ yr⁻¹ and 1.8 kg N ha⁻¹ yr⁻¹, respectively. Relative
432 large declines would be found in their respective hotspots (Case 1-Base, Figures 2e-f).
433 In contrast, a growth of OXN deposition would appear under the SSP5-8.5 pathway,
434 contributed mainly by wet deposition. The changes of dry deposition would be limited
435 within 1 kg N ha⁻¹ yr⁻¹ at the national level (Case 2-Base, Figures 2i-2j). For RDN
436 deposition, there would be a nationwide decline in the 2060s under SSP2-4.5 pathway
437 (Case 1-Base, Figures 2g-h). Large decline would be found for wet deposition in the
438 SCB and the surrounding area, with the maximum exceeding 10 kg N ha⁻¹ yr⁻¹. The
439 changes under the SSP5-8.5 pathway would be small, with the national average reduced
440 by 0.1 and 0.5 kg N ha⁻¹ yr⁻¹ for dry and wet deposition, respectively (Case 2-Base,
441 Figures 2k-l).

442 With Cases 3 and 4 included in the analyses, we further estimated the impacts of
443 climate and emission change on future total Nr deposition and compared them with the
444 joint impact (Figure 3). Under the SSP2-4.5 pathway, the national average difference
445 in Nr deposition due to changing emissions alone (-5.48 kg N ha⁻¹ yr⁻¹, Figure 3b) was
446 closer to that from joint impacts (-5.77 kg N ha⁻¹ yr⁻¹, Figure 3c), while the difference



447 caused by climate change alone was small ($-0.29 \text{ kg N ha}^{-1} \text{ yr}^{-1}$, Figure 3a). Additionally,
448 the spatial correlation (R) between the difference in deposition due to emission change
449 alone and that due to both factors would be 0.89 (Figure 3b), while it would be clearly
450 smaller at 0.66 between those due to climate change alone and both factors (Figure 3a).
451 This indicates that the future long-term Nr deposition would be primarily dominated by
452 emission change. Under the SSP5-8.5 pathway, the total amount of Nr deposition
453 change at the national level would also be dominated by the varying emissions. The
454 emission change alone would lead to a growth of nationwide deposition at 0.83 kg N
455 $\text{ha}^{-1} \text{ yr}^{-1}$ (Figure 3e), 90% of the total growth ($0.92 \text{ kg N ha}^{-1} \text{ yr}^{-1}$, Figure 3f). However,
456 the spatial pattern of deposition would be largely modulated by climate change, with
457 the spatial R between the deposition differences due to climate change alone and both
458 factors reaching 0.84 (Figure 3d). The value would only be 0.55 between differences
459 due to emission change alone and both factors (Figure 3e). In the southern BTH, for
460 example, future climate change would elevate the deposition by over $4 \text{ kg N ha}^{-1} \text{ yr}^{-1}$.
461 By comparing the roles of emission and climate changes in Nr deposition under
462 different SSP-RCP pathways, our study emphasizes that the rigorous implementation
463 of emission controls in the future can effectively mitigate the adverse perturbations of
464 climate change.

465 **3.3 Varying effects of different emission changing patterns on Nr** 466 **deposition**

467 We further quantified the effects of emission controls on the deposition of different
468 Nr components (OXN and RDN) and compared them under various future emission
469 scenarios (“Baseline”, “Current-goal”, and “Neutral-goal”). As illustrated in Figure 4,
470 with an exception of OXN deposition in “Baseline” scenario which would increase 24%
471 ($1.42 \text{ kg N ha}^{-1} \text{ yr}^{-1}$) from 2010s to 2060s, the national Nr deposition would commonly
472 decline for other cases, ranging from 5% to 85% ($0.27\text{-}4.93 \text{ kg N ha}^{-1} \text{ yr}^{-1}$). In the
473 “Neutral-goal” scenario, in particular, the national average OXN deposition was
474 predicted to decline to $0.98 \text{ kg N ha}^{-1} \text{ yr}^{-1}$ by 2060s (Figure S4), accounting for only



475 17% of the total Nr deposition. This implies that the continuous and substantial
476 reduction in NO_x emissions, implemented as part of the national strategy to address
477 climate change and to improve air quality, would make RDN become the dominant
478 contributor to future Nr deposition. Spatial correlation between future emission change
479 and the resulting deposition change was estimated and summarized in Table S2 in the
480 supplement for different emission scenarios. Compared with OXN, the spatial change
481 in RDN deposition would be more consistent with that of precursor emissions, indicated
482 by a much higher R for RDN (0.67-0.72) than OXN (0.24-0.35). The discrepancy could
483 result from the stronger regional transport of NO_x, which comes largely from high-stack
484 sources (Ma et al., 2020).

485 Figure 5 compares the relative changes in future Nr deposition and precursor
486 emissions for WC and EC in different emission scenarios. Under the “Baseline”
487 scenario (Figure 5a), the OXN deposition in WC was predicted to increase 47% from
488 2010s to 2060s. This growth would be notably smaller than that of NO_x emissions
489 (81%), suggesting that a larger amount of OXN in WC would deposit to the east through
490 atmospheric transport. However, the transport might be weakened from WC to EC in
491 the “Current-goal” (Figure 5b) and “Neutral-goal” scenarios (Figure 5c), in which the
492 OXN deposition in WC would decline (46% and 85%, respectively) greater than that
493 of NO_x emissions (41% and 77%, respectively). Additional experiments were
494 conducted to quantify the impact of changing transport from WC on deposition in EC,
495 by keeping the emissions in WC at the 2010s levels (Cases 6-8). The fluxes crossing
496 110°E from west to east were calculated within the altitude from the surface to 100 hpa
497 and latitude from 20°N to 50°N. Compared to the cases where emissions in WC were
498 maintained at the 2010 levels, the outflow fluxes of OXN would change by 17.57 (Case
499 2-Case 7), -20.10 (Case 1-Case 6) and -37.12 kg N s⁻¹ (Case 5-Case 8) for “Baseline”,
500 “Current-goal” and “Neutral-goal” scenarios, respectively (Table S3). Consequently,
501 the OXN deposition in EC would change by 0.30 (2%), -0.28 (-5%), and -0.51 kg N ha⁻¹
502 yr⁻¹ (-27%) from 2010s to 2060s due to the emission variation in WC for different
503 scenarios (Table 4).



504 The OXN deposition in EC was predicted to increase 13%, despite a 17% growth
505 in NO_x emissions under the “Baseline” scenario (Figure 5a). The additional deposition
506 loss may have been exported off-land through long-distance transport processes. Zhao
507 et al. (2017) demonstrated that 30% of China’s Nr emissions from 2008-2010 were
508 transported to the China Sea Area of the Northwest Pacific. We calculated the outflow
509 fluxes of OXN from EC crossing 123°E within the altitude from the surface to 100hpa
510 and latitude from 20°N to 50°N (Table S4). Under the “Baseline” scenario, the outflow
511 fluxes from EC in 2060s would increase by $34.56 \text{ kg N s}^{-1}$ compared to the case with
512 the emissions maintained at the 2010s level (Case 2-Case 4). In contrast, the outflow
513 fluxes under the “Current-goal” and “Neutral-goal” scenarios would respectively
514 decline by 94.45 (Case 1-Case 3) and $172.86 \text{ kg N s}^{-1}$ (Case 5-Case 3) attributable to
515 the emission abatement in EC, making the relative changes in NO_x emissions and OXN
516 deposition would be essentially equal. The result implies that effective implementation
517 of China’s clean air and carbon neutrality policies would definitely weaken its role of
518 exporting pollution to west Pacific.

519 For RDN deposition, the relative change in emissions and deposition would be
520 essentially the same under the “Baseline” scenario (Figure 5a). However, the change in
521 RDN deposition would be smaller than that of NH_3 emissions for both EC and WC in
522 the remaining two scenarios (Figure 5b and 5c). Given its short atmospheric lifetime
523 (generally a few hours) and thereby limited long-distance transport capability (Hertel
524 et al., 2006), the lag in RDN deposition reduction could primarily result from chemical
525 transformation processes. As a crucial reduced gas in the atmosphere, NH_3 exhibits high
526 capability of neutralizing acid gases, thereby slowing down the formation of acid rain
527 and actively participating in the production of sulfates (SO_4^{2-}) and NO_3^- . With the
528 substantial reduction in acidic pollutants, the secondary formation of ammonium sulfate
529 and ammonium nitrate aerosols would decline, leading to an enhanced proportion of
530 gaseous NH_3 in RDN. Given much larger V_d of gaseous NH_3 than that of particulate
531 NH_4^+ , the enhanced NH_3 would result in a growth in dry deposition of RDN, thus
532 slowing the decline of total RDN deposition.



533 **3.4 Responses of future Nr deposition to emission perturbation**

534 Figure 6 shows the predicted response of Nr deposition to a 20% emission
535 reduction for 2010s and 2060s under different emission scenarios. The response was
536 obtained by calculating the ratio of the percent change in deposition to that in emissions.
537 For OXN, the nationwide average response of OXN deposition to NO_x emissions was
538 83% for the 2010s (Figure 6a). There was a clear north-south difference in the response
539 over EC. We defined Northern China (NC, 30°N-45°N, 110°E-125°E) and Southern
540 China (SC, 20°N-30°N, 110°E-125°E, Figure S1) and calculated the response of OXN
541 deposition to NO_x emission change at 83% and 96%, respectively (Table 5). As a
542 comparison, Liu et al. (2022) reported the response of OXN deposition to NO_x
543 emissions ranging 55-76% in North China Plain and neighboring areas during the 2010s.
544 High ratio of NO_x to VOCs emissions in NC resulted in the NO_x-saturated regime for
545 O₃ formation, and reduced NO_x emissions enhanced the atmospheric oxidation capacity
546 (AOC) and in turn promoted the production of atmospheric nitric acid (HNO₃).
547 Additionally, there was insufficient ambient free NH₃ to completely neutralize the
548 gaseous HNO₃, an important component of OXN_DDEP (Liu et al., 2018; Zhai et al.,
549 2021). The relatively large proportion of HNO₃ in OXN restrained fast decline of
550 OXN_DDEP, given the larger V_d of HNO₃ compared to that of NO₂. Overall, the
551 enhanced AOC, coupled with relatively NH₃-poor condition, resulted in a weak
552 response of OXN deposition to emissions reduction. In our simulations, emissions were
553 controlled for all species including VOCs. Compared to Liu et al. (2022) with NO_x
554 emission reduction only, the extra VOCs emissions reduction might lower AOC due to
555 their great contribution to the formation of O₃ and OH radicals in the atmosphere
556 (McDonald et al., 2018). Thus, the moderately large response in our simulation resulted
557 from the simultaneous reduction of VOC and NO_x emissions, which would partially
558 offset the AOC enhancement induced by NO_x emission control alone, and thereby
559 restrain the OXN deposition to some extent.

560 Similar to the 2010s, the response of OXN deposition to a 20% emission reduction
561 in the 2060s would be 84% over NC under the “Baseline” scenario, in which VOCs and



562 NO_x emissions would remain high levels (Table 5). A 20% reduction in emissions
563 would lead to a 17% decline in near-surface annual mean NO₂ concentrations (Figure
564 S5a in the supplement) but a 3.2% growth in O₃ concentration in NC (Figure S5b). In
565 contrast, under the scenarios of “Current-goal” and “Neutral-goal”, a 20% emission
566 reduction would result in 0.82% and 2.7% decline in near-surface O₃ concentration,
567 respectively (Figure S5b), indicating a weakening non-linear mechanism between
568 emission reduction and AOC enhancement with long-term control of air pollution.
569 Meanwhile, the annual mean HNO₃ concentrations would decrease by 14% and 19%
570 (Figure S5c), and OXN_DDEP would decrease by 18% and 19% (Figure S5d) in
571 “Current-goal” and “Neutral-goal” scenarios, respectively. The reductions would be
572 greater than those for the historical period and the future “Baseline” scenario (10% and
573 11% for HNO₃ concentration and 14% and 14% for OXN_DDEP, respectively).
574 Consequently, the response of total OXN deposition to emission controls would reach
575 92% and 95%, respectively. Compared to NC, greater effectiveness of emission
576 abatement on decreasing OXN deposition was found in SC for both 2010s and all the
577 future scenarios in 2060s. The response was estimated to range 93%-103.00% (Table
578 5), similar to the results of 80-120% in the United States (Tan et al., 2020).

579 The response of RDN deposition to a 20% reduction of emissions was estimated
580 at 96% in 2010s, clearly larger than that in the United States (60-80%, Tan et al., 2020).
581 The value would decline to 94% and 92% for “Current-goal” and “Neutral-goal”
582 scenarios in 2060s, respectively, implying that the national air quality and carbon
583 neutrality policies would enhance the nonlinear response of RDN deposition to
584 precursor emission change, towards current US condition. As mentioned in previously,
585 part of the reason could be the transition to a more NH₃-rich condition in the future,
586 resulting from more stringent emission controls of SO₂ and NO_x than NH₃. The
587 proportion of gaseous NH₃ (with larger V_d than particulate NH₄⁺) to total RDN would
588 be enhanced, which would in turn delay the reducing RDN deposition. In addition, our
589 simulations did not account for the bidirectional feedback between atmospheric NH₃
590 and soil. Soil volatilization could weaken the sensitivity of dry deposition of RDN to



591 changing NH₃ emissions.

592 **4 Conclusion remarks**

593 Combining two global SSP-RCP climate change pathways and three Chinese
594 emission control scenarios, we assessed the spatiotemporal evolution of future
595 atmospheric Nr deposition in China, its main driving factors, and the changing response
596 of Nr deposition to precursor emission controls. Under the SSP5-8.5 pathway, the total
597 Nr deposition would increase from 14.7 in 2010s to 15.4 kg N ha⁻¹ yr⁻¹ in 2060s, and
598 the spatial pattern of deposition would largely be modulated by climate change. In
599 contrast, under the SSP2-4.5 pathway, Nr deposition is predicted to decrease to 9.0 kg
600 N ha⁻¹ yr⁻¹ by the 2060s, strongly driven by emissions changes. Implementation of
601 clean air and carbon neutrality policies would make RDN become the dominant
602 contributor to future Nr deposition. In the “Neutral-goal” scenario, in particular, the
603 national average OXN deposition was predicted to decrease to 0.98 kg N ha⁻¹ yr⁻¹ by
604 the 2060s, accounting for only 17% of the total Nr deposition. Previous studies at the
605 global scale have also indicated the increasing role of RDN deposition in the future, but
606 the growth of RDN share was commonly predicted to be slower, due to insufficient
607 knowledge on China’s actions on NO_x emission controls. For example, ACCMIP, as
608 reported by Sun et al. (2020), expected that the ratio of RDN to total Nr deposition in
609 eastern China will increase to only 56% by the end of the century.

610 Through experiments with fixed WC emissions, we further revealed that the OXN
611 deposition from WC to EC in the 2060s would increase by 0.30 kg N ha⁻¹ yr⁻¹ (2%)
612 compared to the 2010s under the “Baseline”, but decline by 0.28 kg N ha⁻¹ yr⁻¹ (5%)
613 and 0.51 kg N ha⁻¹ yr⁻¹ (27%) under the “Current-goal” and “Neutral-goal” scenarios,
614 respectively. Similarly, the outflow OXN fluxes from EC in 2060s would decline 94.45
615 kg N s⁻¹ (49%) and 172.86 kg N s⁻¹ (89%) in the latter two scenarios in 2060s,
616 respectively. The response of OXN deposition to a 20% abatement of emissions in NC
617 was estimated at 84% under the “Baseline” scenario, while it would approach 100% in
618 the “Current-goal” and “Neutral-goal” scenarios with the declining share of gaseous



619 HNO_3 in OXN due to weakened AOC. In contrast, the response of RDN deposition to
620 a 20% abatement of emissions would decline in the latter two scenarios, attributed
621 partly to a more NH_3 -rich condition and thereby a growing share of gaseous NH_3 in
622 2060s.

623 Our study suggests that future rigorous implementation of clean air and carbon
624 neutrality policies can mitigate the adverse effects of climate change on Nr deposition,
625 and weaken the transport of air pollution to West Pacific. It highlights the potential
626 changes in the source-sink relationship for China, and supports scientific analyses on
627 sources and mitigation of Nr pollution, not only for China but also for downwind areas.
628 More attention needs to be paid to NH_3 emission controls due to its increasing
629 importance on Nr deposition. The sharp decline in future Nr deposition driven by
630 profound emission abatement may substantially reduce the ecological damages like
631 acidification and eutrophication. Meanwhile, it might potentially weaken the carbon
632 sink capacity of terrestrial ecosystems. A comprehensive consideration of the balance
633 between Nr control and terrestrial carbon sinks is essential for the future.

634 Our findings are subject to some limitations. Firstly, given the computationally
635 intensive of numerical simulation, the Nr deposition was simulated with a single model
636 (CMAQ) in this work. As suggested by the MICS-Asia III project, there existed clear
637 difference in Nr deposition simulation among multiple CTMs, and in particular the
638 consistency of dry deposition of OXN was relatively poor, with coefficient of variation
639 (CV) ranging 0.4-0.5 throughout most of China (Ge et al., 2020). Multi-model ensemble
640 methodology is thus recommended in future work to reduce the bias of single-model
641 simulation. Secondly, the role of climate change on future Nr deposition might be
642 underestimated. Climate-driven effects on emissions were not considered in this study,
643 such as the increase of NH_3 volatilization due to global warming (Ren et al., 2023). In
644 addition, we mainly addressed the future evolution of Nr deposition under the mean
645 state of climate, but neglected the potential impact of extreme climatic events. For
646 example, the changing frequency of heavy precipitation was reported as a key factor
647 influencing the variation of Nr deposition (Chen et al., 2023). Therefore, more analyses



648 should be conducted on the connection between the changing extreme climate events
649 and atmospheric deposition.

650 **Data availability**

651 All data in this study are available from the authors upon request.

652 **Author contributions**

653 MMA developed the strategy and methodology of the work and wrote the draft. Y
654 Zhao improved the methodology and revised the manuscript. JCao provided useful
655 comments on the paper. BZheng provided the historical emission inventory. DTong
656 provided the future emission inventory.

657 **Competing interests**

658 The authors declare that they have no conflict of interest.

659 **Acknowledgments**

660 This work was sponsored by National Key Research and Development Program of
661 China (2023YFC3709802) and the National Natural Science Foundation of China
662 (42177080). We are grateful to the High Performance Computing Center (HPCC) of
663 Nanjing University for doing the numerical calculations in this paper on its blade cluster
664 system. We would also like to thank Tsinghua University for the free use of national
665 emissions data (MEIC and DPEC), European Weather Forecasting Center for the free
666 download of meteorological reanalysis data.

668 **References**

669 Appel, W., Napelenok, S., Hogrefe, C., Pouliot, G., Foley, K., Roselle, S., Pleim, J.,
670 Bash, J., Pye, H., Heath, N., Murphy, B., & Mathur, R. (2017). Overview and



- 671 Evaluation of the Community Multiscale Air Quality (CMAQ) Modeling System
672 Version 5.2. Chapter 11, Air Pollution Modeling and its Application XXV.
673 Springer International Publishing AG, Cham (ZG), Switzerland, 69-73.
674 https://doi.org/10.1007/978-3-319-57645-9_11
- 675 Bey, I., Jacob, D. J., Yantosca, R. M., Logan, J. A., Field, B. D., Fiore, A. M., Li, Q.,
676 Liu, H. Y., Mickley, L. J., & Schultz, M. G. (2001). Global modeling of
677 tropospheric chemistry with assimilated meteorology: Model description and
678 evaluation. *Journal of Geophysical Research: Atmospheres*, 106(D19), 23073-
679 23095. <https://doi.org/10.1029/2001JD000807>
- 680 Carvalho, D., Rocha, A., Gómez-Gesteira, M., & Santos, C. (2012). A sensitivity study
681 of the WRF model in wind simulation for an area of high wind energy.
682 *Environmental Modelling & Software*, 33, 23–34.
683 <https://doi.org/10.1016/j.envsoft.2012.01.019>
- 684 Chang, J. S., Brost, R. A., Isaksen, I. S. A., Madronich, S., Middleton, P., Stockwell, W.
685 R., & Walcek, C. J. (1987). A three-dimensional Eulerian acid deposition model:
686 Physical concepts and formulation. *Journal of Geophysical Research:*
687 *Atmospheres*, 92(D12), 14681-14700. <https://doi.org/10.1029/JD092iD12p14681>
- 688 Chang, M., Cao, J., Ma, M., Liu, Y., Liu, Y., Chen, W., Fan, Q., Liao, W., Jia, S., &
689 Wang, X. (2020). Dry deposition of reactive nitrogen to different ecosystems
690 across eastern China: A comparison of three community models. *Science of The*
691 *Total Environment*, 720, 137548. <https://doi.org/10.1016/j.scitotenv.2020.137548>
- 692 Chang, Y., Huang, R. J., Ge, X., Huang, X., Hu, J., Duan, Y., Zou, Z., Liu, X., &
693 Lehmann, M. F. (2020). Puzzling haze events in China during the coronavirus
694 (COVID-19) shutdown. *Geophysical Research Letters*, 47(12), e2020GL088533.
695 <https://doi.org/10.1029/2020GL088533>
- 696 Chen, C., Xiao, W., & Chen, H. Y. (2023). Mapping global soil acidification under N
697 deposition. *Global Change Biology*, 29(16), 4652-4661.
698 <https://doi.org/10.1111/gcb.16813>



- 699 Chen, Y., Zhang, L., Henze, D. K., Zhao, Y., Lu, X., Winiwarter, W., Guo, Y., Liu, X.,
700 Wen, Z., & Song, Y. (2021). Interannual variation of reactive nitrogen emissions
701 and their impacts on PM_{2.5} air pollution in China during 2005–2015.
702 Environmental Research Letters, 16(12), 125004. <https://doi.org/10.1088/1748-9326/ac3695>
703
- 704 Cheng, F. Y., Feng, C. Y., Yang, Z. M., Hsu, C. H., Chan, K. W., Lee, C. Y., & Chang,
705 S. C. (2021). Evaluation of real-time PM_{2.5} forecasts with the WRF-CMAQ
706 modeling system and weather-pattern-dependent bias-adjusted PM_{2.5} forecasts in
707 Taiwan. Atmospheric Environment, 244, 117909.
708 <https://doi.org/10.1016/j.atmosenv.2020.117909>
- 709 Cheng, J., Tong, D., Liu, Y., Geng, G., Davis, S. J., He, K., & Zhang, Q. (2023). A
710 synergistic approach to air pollution control and carbon neutrality in China can
711 avoid millions of premature deaths annually by 2060. One Earth, 6(8), 978-989.
712 <https://doi.org/10.1016/j.oneear.2023.07.007>
- 713 Cheng, J., Tong, D., Liu, Y., Yu, S., Yan, L., Zheng, B., Geng, G., He, K., & Zhang, Q.
714 (2021a). Comparison of current and future PM_{2.5} air quality in China under
715 CMIP6 and DPEC emission scenarios. Geophysical Research Letters, 48(11),
716 e2021GL093197. <https://doi.org/10.1029/2021GL093197>
- 717 Cheng, J., Tong, D., Zhang, Q., Liu, Y., Lei, Y., Yan, G., Yan, L., Yu, S., Cui, R. Y.,
718 Clarke, L., Geng, G. N., Zheng, B., Zhang, X. Y., Davis, J. S., & He, K. B. (2021b).
719 Pathways of China's PM_{2.5} air quality 2015–2060 in the context of carbon
720 neutrality. National Science Review, 8(12), nwab078.
721 <https://doi.org/10.1093/nsr/nwab078>
- 722 Chen, W., Jia, S., Wang, X., Shao, M., Liao, W., Guenther, A., Flechard, C., Yu, P.,
723 Zhong, B., Chang, M., Wang, W., Mao, J., Liu, X., Yu, G., & Carmichael, G.
724 (2023). Precipitation trend increases the contribution of dry reduced nitrogen
725 deposition. npj Climate and Atmospheric Science, 6(1), 62.
726 <https://doi.org/10.1038/s41612-023-00390-7>
- 727 Cook, B. I., Mankin, J. S., Marvel, K., Williams, A. P., Smerdon, J. E., & Anchukaitis,



- 728 K. J. (2020). Twenty-first century drought projections in the CMIP6 forcing
729 scenarios. *Earth's Future*, 8(6), e2019EF001461.
730 <https://doi.org/10.1029/2019EF001461>
- 731 De Meij, A., & Vinuesa, J. F. (2014). Impact of SRTM and Corine Land Cover data on
732 meteorological parameters using WRF. *Atmospheric Research*, 143, 351-370.
733 <https://doi.org/10.1016/j.atmosres.2014.03.004>
- 734 Dong, L., Miao, G., & Wen, W. (2021). China's carbon neutrality policy: Objectives,
735 impacts and paths. *East Asian Policy*, 13(01), 5-18.
736 <https://doi.org/10.1142/S1793930521000015>
- 737 Ellis, R. A., Jacob, D. J., Sulprizio, M. P., Zhang, L., Holmes, C. D., Schichtel, B. A.,
738 Blett, T., Porter, E., Pardo, L. H., & Lynch, J. A. (2013). Present and future
739 nitrogen deposition to national parks in the United States: critical load exceedances.
740 *Atmospheric Chemistry and Physics*, 13(17), 9083–9095.
741 <https://doi.org/10.5194/acp-13-9083-2013>
- 742 Fowler, D., Coyle, M., Skiba, U., Sutton, M. A., Cape, J. N., Reis, S., Sheppard, L. J.,
743 Jenkins, A., Grizzetti, B., Galloway, J. N., Vitousek, P., Leach, A., Bouwman, A.
744 F., Butterbach-Bahl, K., Dentener, F., Stevenson, D., Amann, M., & Voss, M.
745 (2013). The global nitrogen cycle in the twenty-first century. *Philosophical*
746 *Transactions of the Royal Society B: Biological Sciences*, 368(1621), 20130164.
747 <https://doi.org/10.1098/rstb.2013.0164>
- 748 Gao, Q., Zhang, X., Liu, L., Lu, X., & Wang, Y. (2023). A database of atmospheric
749 inorganic nitrogen deposition fluxes in China from satellite monitoring. *Scientific*
750 *Data*, 10(1), 698. <https://doi.org/10.1038/s41597-023-02607-z>
- 751 Galloway, J. N., Dentener, F. J., Capone, D. G., Boyer, E. W., Howarth, R. W.,
752 Seitzinger, S. P., Asner, G. P., Cleveland, C. C., Green, P. A., Holland, E. A., Karl,
753 D. M., Michaels, A. F., Porter, J. H., Townsend, A. R., & Vöosmarty, C. J. (2004).
754 Nitrogen cycles: past, present, and future. *Biogeochemistry*, 70, 153-226.
755 <https://doi.org/10.1007/s10533-004-0370-0>
- 756 Ge, B., Itahashi, S., Sato, K., Xu, D., Wang, J., Fan, F., Tan, Q., Fu, J. S., Wang, X.,



- 757 Yamaji, K., Nagashima, T., Li, J., Kajino, M., Liao, H., Zhang, M., Wang, Z., Li,
758 M., Woo, J. H., Kurokawa, J., Pan, Y., Wu, Q., Liu, X., & Wang, Z. (2020). Model
759 Inter-Comparison Study for Asia (MICS-Asia) phase III: multimodel comparison
760 of reactive nitrogen deposition over China. *Atmospheric Chemistry and Physics*,
761 20(17), 10587–10610. <https://doi.org/10.5194/acp-20-10587-2020>
- 762 Guenther, A., Jiang, X., Heald, C. L., Sakulyanontvittaya, T., Duhl, T., Emmons, L. K.,
763 & Wang, X. (2012). The Model of Emissions of Gases and Aerosols from Nature
764 version 2.1 (MEGAN2.1): an extended and updated framework for modeling
765 biogenic emissions. *Geoscientific Model Development*, 5(6), 1471-1492.
766 <https://doi.org/10.5194/gmd-5-1471-2012>
- 767 Han, X., Zhang, M., Skorokhod, A., & Kou, X. (2017). Modeling dry deposition of
768 reactive nitrogen in China with RAMS-CMAQ. *Atmospheric Environment*, 166,
769 47-61. <https://doi.org/10.1016/j.atmosenv.2017.07.015>
- 770 Hertel, O., Skjøth, C. A., Løfstrøm, P., Geels, C., Frohn, L. M., Ellermann, T., &
771 Madsen, P. V. (2006). Modelling Nitrogen Deposition on a Local Scale—A
772 Review of the Current State of the Art. *Environmental Chemistry*, 3(5), 317.
773 <https://doi.org/10.1071/EN06038>
- 774 Hersbach, H., Bell, B., Berrisford, P., Hirahara, S., Horányi, A., Muñoz-Sabater, J.,
775 Nicolas, J., Peubey, C., Radu, R., Schepers, D., Simmons, A., Soci, C., Abdalla,
776 S., Abellan, X., Balsamo, G., Bechtold, P., Biavati, G., Bidlot, J., Bonavita, M., De
777 Chiara, G., Dahlgren, P., Dee, D., Diamantakis, M., Dragani, R., Flemming, J.,
778 Forbes, R., Fuentes, M., Geer, A., Haimberger, L., Healy, S., Hogan, R. J., Hólm,
779 E., Janisková, M., Keeley, S., Laloyaux, P., Lopez, P., Lupu, C., Radnoti, G., de
780 Rosnay, P., Rozum, I., Vamborg, F., Villaume, S., & Thépaut, J. -N. (2020).
781 *Quarterly Journal of the Royal Meteorological Society*, 146(730), 1999-2049.
782 <https://doi.org/10.1002/qj.3803>
- 783 Huang, X., Swain, D. L., & Hall, A. D. (2020). Future precipitation increase from very
784 high resolution ensemble downscaling of extreme atmospheric river storms in
785 California. *Science advances*, 6(29), eaba1323.



- 786 <https://doi.org/10.1126/sciadv.aba1323>
- 787 IPCC, 2021. Climate Change 2021: The Physical Science Basis. Contribution of
788 Working Group I to the Sixth Assessment Report of the Intergovernmental Panel
789 on Climate Change, Cambridge.
- 790 Kanakidou, M., Myriokefalitakis, S., Daskalakis, N., Fanourgakis, G., Nenes, A., Baker,
791 A. R., Tsigaridis, K., & Mihalopoulos, N. (2016). Past, Present, and Future
792 Atmospheric Nitrogen Deposition. *Journal of the Atmospheric Sciences*, 73(5),
793 2039–2047. <https://doi.org/10.1175/JAS-D-15-0278.1>
- 794 Kawase, H., Hara, M., Yoshikane, T., Ishizaki, N. N., Uno, F., Hatsushika, H., & Kimura,
795 F. (2013). Altitude dependency of future snow cover changes over Central Japan
796 evaluated by a regional climate model. *Journal of Geophysical Research:
797 Atmospheres*, 118(22), 12-444. <https://doi.org/10.1002/2013JD020429>
- 798 Kang, Y., Liu, M., Song, Y., Huang, X., Yao, H., Cai, X., Zhang, H., Kang, L., Liu, X.,
799 Yan, X., He, H., Zhang, Q., Shao, M., & Zhu, T. (2016). High-resolution ammonia
800 emissions inventories in China from 1980 to 2012. *Atmospheric Chemistry and
801 Physics*, 16(4), 2043–2058. <https://doi.org/10.5194/acp-16-2043-2016>
- 802 Kim, J. E., Han, Y. J., Kim, P. R., & Holsen, T. M. (2012). Factors influencing
803 atmospheric wet deposition of trace elements in rural Korea. *Atmospheric
804 Research*, 116, 185-194. <https://doi.org/10.1016/j.atmosres.2012.04.013>
- 805 Koetse, M. J., & Rietveld, P. (2009). The impact of climate change and weather on
806 transport: An overview of empirical findings. *Transportation Research Part D:
807 Transport and Environment*, 14(3), 205-221.
808 <https://doi.org/10.1016/j.trd.2008.12.004>
- 809 Lamarque, J. -F., Dentener, F., McConnell, J., Ro, C. -U., Shaw, M., Vet, R., Bergmann,
810 D., Cameron-Smith, P., Dalsoren, S., Doherty, R., Faluvegi, G., Ghan, S. J., Josse,
811 B., Lee, Y. H., MacKenzie, I. A., Plummer, D., Shindell, D. T., Skeie, R. B.,
812 Stevenson, D. S., Strode, S., Zeng, G., Curran, M., Dahl-Jensen, D., Das, S.,
813 Fritzsche, D., & Nolan, M. (2013a). Multi-model mean nitrogen and sulfur
814 deposition from the Atmospheric Chemistry and Climate Model Intercomparison



815 Project (ACCMIP): evaluation of historical and projected future changes.
816 Atmospheric Chemistry and Physics, 13(16), 7997–8018.
817 <https://doi.org/10.5194/acp-13-7997-2013>

818 Lamarque, J.-F., Shindell, D. T., Josse, B., Young, P. J., Cionni, I., Eyring, V.,
819 Bergmann, D., Cameron-Smith, P., Collins, W. J., Doherty, R., Dalsoren, S.,
820 Faluvegi, G., Folberth, G., Ghan, S. J., Horowitz, L. W., Lee, Y. H., MacKenzie,
821 I. A., Nagashima, T., Naik, V., Plummer, D., Righi, M., Rumbold, S. T., Schulz,
822 M., Skeie, R. B., Stevenson, D. S., Strode, S., Sudo, K., Szopa, S., Voulgarakis,
823 A., & Zeng, G. (2013b). The Atmospheric Chemistry and Climate Model
824 Intercomparison Project (ACCMIP): overview and description of models,
825 simulations and climate diagnostics. *Geoscientific Model Development*, 6(1),
826 179–206. <https://doi.org/10.5194/gmd-6-179-2013>

827 Lauer, A., Zhang, C., Elison-Timm, O., Wang, Y., & Hamilton, K. (2013). Downscaling
828 of climate change in the Hawaii region using CMIP5 results: On the choice of the
829 forcing fields. *Journal of Climate*, 26(24), 10006-10030.
830 <https://doi.org/10.1175/JCLI-D-13-00126.1>

831 Li, M., Liu, H., Geng, G., Hong, C., Liu, F., Song, Y., Tong, D., Zheng, B., Cui, H.,
832 Man, H., Zhang, Q., & He, K. (2017). Anthropogenic emission inventories in
833 China: a review. *National Science Review*, 4(6), 834-866.
834 <https://doi.org/10.1093/nsr/nwx150>

835 Li, M., Zhang, Q., Kurokawa, J. -I., Woo, J. -H., He, K., Lu, Z., Ohara, T., Song, Y.,
836 Streets, D. G., Carmichael, G. R., Cheng, Y., Hong, C., Huo, H., Jiang, X., Kang,
837 S., Liu, F., Su, H., and Zheng, B. (2017). MIX: a mosaic Asian anthropogenic
838 emission inventory under the international collaboration framework of the MICS-
839 Asia and HTAP. *Atmospheric Chemistry and Physics*, 17(2), 935-963.
840 <https://doi.org/10.5194/acp-17-935-2017>

841 Liao, J., Wang, T., Jiang, Z., Zhuang, B., Xie, M., Yin, C., Wang, X., Zhu, J., Fu, Y.,
842 & Zhang, Y (2015). WRF/Chem modeling of the impacts of urban expansion on
843 regional climate and air pollutants in Yangtze River Delta, China. *Atmospheric*



844 Environment, 106, 204-214. <https://doi.org/10.1016/j.atmosenv.2015.01.059>

845 Liu, L., Zhang, X., Xu, W., Liu, X., Zhang, Y., Li, Y., Wei, J., Lu, X., Wang, S., Zhang,
846 W., Zhao, L., Wang, Z., & Wu, X. (2020). Fall of oxidized while rise of reduced
847 reactive nitrogen deposition in China. *Journal of Cleaner Production*, 272, 122875.
848 <https://doi.org/10.1016/j.jclepro.2020.122875>

849 Liu, M., Huang, X., Song, Y., Xu, T., Wang, S., Wu, Z., Hu, M., Zhang, L., Zhang, Q.,
850 Pan, Y., Liu, X., & Zhu, T. (2018). Rapid SO₂ emission reductions significantly
851 increase tropospheric ammonia concentrations over the North China Plain.
852 *Atmospheric Chemistry and Physics*, 18, 17933-17943.
853 <https://doi.org/10.5194/acp-18-17933-2018>

854 Liu, M., Shang, F., Lu, X., Huang, X., Song, Y., Liu, B., Zhang, Q., Liu X., Cao, J., Xu,
855 T., Wang T., Xu, Z., Xu, W., Liao W., Kang L., Cai, X., Zhang, H, Dai, Y., & Liu,
856 X. (2022). Unexpected response of nitrogen deposition to nitrogen oxide controls
857 and implications for land carbon sink. *Nature Communications*, 13(1), 3126.
858 <https://doi.org/10.1038/s41467-022-30854-y>

859 Liu, S., Xing, J., Wang, S., Ding, D., Cui, Y., & Hao, J. (2021). Health benefits of
860 emission reduction under 1.5° C pathways far outweigh climate-related variations
861 in China. *Environmental Science & Technology*, 55(16), 10957-10966.
862 <https://doi.org/10.1021/acs.est.1c01583>

863 Liu X., Xu W., Duan, L., Du, E., Pan, Y., Lu, X., Zhang, L., Wu, Z., Wang, X., Zhang,
864 Y., Shen, J., Song, L., Feng, Z., Liu, X., Song, W., Tang, A., Zhang, Y., Zhang, X
& Collett, J. L. (2017). Atmospheric nitrogen emission, deposition, and air quality
865 impacts in China: an overview. *Current Pollution Reports*, 3, 65-77.
866 <https://doi.org/10.1007/s40726-017-0053-9>

867

868 Liu, X., Zhang, Y., Han, W., Tang, A., Shen, J., Cui, Z., Vitousek, P., Erisman, J. W.,
869 Goulding, K., Christie, P., Fangmeier, A., & Zhang, F. (2013). Enhanced nitrogen
870 deposition over China. *Nature*, 494(7438), 459-462.
871 <https://doi.org/10.1038/nature11917>

872 Liu, X. H., Zhang, Y., Cheng, S. H, Xing, J., Zhang, Q., Streets, D. G., Yang, C., Wang,



- 873 W. X., & Hao, J. M. (2010). Understanding of regional air pollution over China
874 using CMAQ, part I performance evaluation and seasonal variation. *Atmospheric*
875 *Environment*, 44(20), 2415-2426. <https://doi.org/10.1016/j.atmosenv.2010.03.035>
- 876 Liu Y., & Wang T. (2020) Worsening urban ozone pollution in China from 2013 to
877 2017–Part 1: The complex and varying roles of meteorology. *Atmospheric*
878 *Chemistry and Physics*, 20(11), 6305-6321. [https://doi.org/10.5194/acp-20-6305-](https://doi.org/10.5194/acp-20-6305-2020)
879 [2020](https://doi.org/10.5194/acp-20-6305-2020)
- 880 Ma, M., Zheng, B., Xu, W., Cao, J., Zhou, K., & Zhao, Y. (2023). Trend and Interannual
881 Variations of Reactive Nitrogen Deposition in China During 2008–2017 and the
882 Roles of Anthropogenic Emissions and Meteorological Conditions. *Journal of*
883 *Geophysical Research: Atmospheres*, 128(6), e2022JD037489.
884 <https://doi.org/10.1029/2022JD037489>
- 885 McDonald, B., De Gouw, J., Gilman, J., Jathar, S., Akherati, A., Cappa, C., Jinenez, J.,
886 Le-Taylor, J., Hayes, P., Mckeen, S., Cui, Y., Kim, S., Gentner, D., Isaacman-
887 Vanwertz, G., Goldstein, A., Harley, R., Frost, G., Roberts, J., Ryerson, T., &
888 Trainer, M. (2018). Volatile chemical products emerging as largest petrochemical
889 source of urban organic emissions. *Science*, 359(6377), 760-764.
890 <https://doi.org/10.1126/science.aag0524>
- 891 Murphy, B. N., Woody, M. C., Jimenez, J. L., Carlton, A. M. G., Hayes, P. L., Liu, S.,
892 Ng, N. L., Russell, L. M., Setyan, A., Xu, L., Young, J., Zaveri, R. A., Zhang, Q.,
893 & Pye, H. O. T. (2017). Semivolatile POA and parameterized total combustion
894 SOA in CMAQv5.2: impacts on source strength and partitioning. *Atmospheric*
895 *Chemistry and Physics*, 17(18), 11107-11133. [https://doi.org/10.5194/acp-2017-](https://doi.org/10.5194/acp-2017-11107-2017)
896 [11107-2017](https://doi.org/10.5194/acp-2017-11107-2017)
- 897 O'Neill, B. C., Tebaldi, C., Van Vuuren, D. P., Eyring, V., Friedlingstein, P., Hurtt, G.,
898 Knutti, R., Kriegler, E., Lamarque, J. -F., Lowe, J., Meehl, G. A., Moss, R., Riahi,
899 K & Sanderson, B. M. (2016). The scenario model intercomparison project
900 (ScenarioMIP) for CMIP6. *Geoscientific Model Development*, 9(9), 3461-3482.
901 <https://doi.org/10.5194/gmd-9-3461-2016>



- 902 Pineda, N., Jorba, O., Jorge, J., & Baldasano, J. M. (2004). Using NOAA AVHRR and
903 SPOT VGT data to estimate surface parameters: application to a mesoscale
904 meteorological model. *International journal of remote sensing*, 25(1), 129-143.
905 <https://doi.org/10.1080/0143116031000115201>
- 906 Pye, H. O. T., Murphy, B. N., Xu, L., Ng, N. L., Carlton, A. G., Guo, H., Weber, R.,
907 Vasilakos, P., Appel, K. W., Budisulistiorini, S. H., Surratt, J. D., Nenes, A., Hu,
908 W., Jimenez, J. L., Isaacman-VanWertz, G., Misztal, P. K., & Goldstein, A. H.
909 (2017). On the implications of aerosol liquid water and phase separation for
910 organic aerosol mass. *Atmospheric Chemistry and Physics*, 17(1), 343-369.
911 <https://doi.org/10.5194/acp-17-343-2017>
- 912 Raza, S, Miao, N, Wang, P, Ju, X., Chen, Z., Zhou, J., & Kuzyakov Y. (2020). Dramatic
913 loss of inorganic carbon by nitrogen - induced soil acidification in Chinese
914 croplands. *Global change biology*, 26(6), 3738-3751.
915 <https://doi.org/10.1111/gcb.15101>
- 916 Sarwar, G., Luecken, D.J., Yarwood, G., Whitten, G.D., & Carter, W.P. (2008). Impact
917 of an updated carbon bond mechanism on predictions from the CMAQ modeling
918 system: preliminary assessment. *Journal of Applied Meteorology and Climatology*,
919 47(1), 3-14. <https://doi.org/10.1175/2007JAMC1393.1>
- 920 Shen, A., Liu, Y., Lu, X., Xu, Y., Jin, Y., Wang, H., Zhang, J., Wang, X., Chang, M.,
921 & Fan, Q (2023). Modeling regional nitrogen cycle in the atmosphere: Present
922 situation and its response to the future emissions control strategy. *Science of The*
923 *Total Environment*, 891, 164379. <https://doi.org/10.1016/j.scitotenv.2023.164379>
- 924 Shen, Y., Jiang, F., Feng, S., Zheng, Y., Cai, Z., & Lyu, X. (2021). Impact of weather
925 and emission changes on NO₂ concentrations in China during 2014–2019.
926 *Environmental Pollution*, 269(15), 116163.
927 <https://doi.org/10.1016/j.envpol.2020.116163>
- 928 Shi, X., Zheng, Y., Lei, Y., Xue, W., Yan, G., Liu, X., Cai, B., Tong, D., & Wang, J.
929 (2021). Air quality benefits of achieving carbon neutrality in China. *Science of the*



- 930 Total Environment, 795, 148784. <https://doi.org/10.1016/j.scitotenv.2021.148784>
- 931 Skamarock W C & Klemp J B. (2008). A time-split nonhydrostatic atmospheric model
932 for weather research and forecasting applications. Journal of Computational
933 Physics, 227(7), 3465-3485. <https://doi.org/10.1016/j.jcp.2007.01.037>
- 934 Sun, K., Gao, Y., Guo, X., Zhang, J., Zeng, X., Ma, M., Chen, Y., Luo, K., Yao, X., &
935 Gao, H. (2022). The enhanced role of atmospheric reduced nitrogen deposition in
936 future over East Asia–Northwest Pacific. Science of The Total Environment, 833,
937 155146. <https://doi.org/10.1016/j.scitotenv.2022.155146>
- 938 Tan, J., Fu, J. S., & Seinfeld, J. H. (2020). Ammonia emission abatement does not fully
939 control reduced forms of nitrogen deposition. Proceedings of the National
940 Academy of Sciences, 117(18), 9771–9775.
941 <https://doi.org/10.1073/pnas.1920068117>
- 942 Taniguchi, K., & Tajima, Y. (2020). Variations in extreme wave events near a South
943 Pacific Island under global warming: case study of Tropical Cyclone Tomas.
944 Progress in Earth and Planetary Science, 7(1), 1-16.
945 <https://doi.org/10.1186/s40645-020-0321-y>
- 946 Tong, D., Cheng, J., Liu, Y., Yu, S., Yan, L., Hong, C., Qin, Y., Zhao, H., Zheng, Y.,
947 Geng, G., Li, M., Liu, F., Zhang, Y., Zheng, B., Clarke, L., & Zhang, Q. (2020).
948 Dynamic projection of anthropogenic emissions in China: methodology and 2015–
949 2050 emission pathways under a range of socio-economic, climate policy, and
950 pollution control scenarios, Atmospheric Chemistry and Physics, 20(9), 5729–
951 5757. <https://doi.org/10.5194/acp-20-5729-2020, 2020>
- 952 Wang, X., Tolksdorf, V., Otto, M., & Scherer, D. (2021). WRF -based dynamical
953 downscaling of ERA5 reanalysis data for High Mountain Asia: Towards a new
954 version of the High Asia Refined analysis. International Journal of Climatology,
955 41(1), 743-762. <https://doi.org/10.1002/joc.6686>
- 956 Ummerhofer, C. C., & Meehl, G. A. (2017). Extreme weather and climate events with
957 ecological relevance: a review. Philosophical Transactions of the Royal Society B:
958 Biological Sciences, 372(1723), 20160135.



- 959 <https://doi.org/10.1098/rstb.2016.0135>
- 960 Van Vuuren, D. P., Edmonds, J., Kainuma, M., Riahi, K., Thomson, A., Hibbard, K.,
961 Hurtt, G. C., Kram, T., Krey, V., Lamarque, J. F., Masui, T., Meinshausen, M.,
962 Nakicenovic, N., Smith, S. J., & Rose, S. K. (2011). The representative
963 concentration pathways: an overview. *Climatic Change*, 109, 5-31.
964 <https://doi.org/10.1007/s10584-011-0148-z>
- 965 Vet, R., Artz, R. S., Carou, S., Shaw, M., Ro, C.-U., Aas, W., Baker, A., Bowersox, V.
966 C., Dentener, F., Galy-Lacaux, C., Hou, A., Pienaar, J. J., Gillett, R., Forti, M. C.,
967 Gromov, S., Hara, H., Khodzher, T., Mahowald, N. M., Nickovic, S., Rao, P. S.
968 P., & Reid, N. W. (2014). A global assessment of precipitation chemistry and
969 deposition of sulfur, nitrogen, sea salt, base cations, organic acids, acidity and pH,
970 and phosphorus. *Atmospheric Environment*, 93, 3–100.
971 <https://doi.org/10.1016/j.atmosenv.2013.10.060>
- 972 Venkatram, A., & Pleim, J. (1999). The electrical analogy does not apply to modeling
973 dry deposition of particles. *Atmospheric Environment*, 33(18), 3075-3076.
974 [https://doi.org/10.1016/S1352-2310\(99\)00094-1](https://doi.org/10.1016/S1352-2310(99)00094-1)
- 975 Wen, Z., Xu, W., Li, Q., Han, M., Tang, A., Zhang, Y., Luo, X., Shen, J., Wang, W.,
976 Li, K., Pan, Y., Zhang, L., Li, W., Collett Jr, J. L., Zhong, B., Wang, X., Goulding,
977 K., Zhang, F., & Liu, X. (2020). Changes of nitrogen deposition in China from
978 1980 to 2018. *Environment International*, 144, 106022.
979 <https://doi.org/10.1016/j.envint.2020.106022>
- 980 Wesely, M. L. (2007). Parameterization of surface resistances to gaseous dry deposition
981 in regional-scale numerical models. *Atmospheric Environment*, 41, 52-63.
982 <https://doi.org/10.1016/j.atmosenv.2007.10.058>
- 983 Wu, Z., Schwede, D. B., Vet, R., Walkr, J. T., Shaw, Mike., Staebler, R., & Zhang, L.
984 (2018). Evaluation and Intercomparison of Five North American Dry Deposition
985 Algorithms at a Mixed Forest Site. *Journal of Advances in Modeling Earth*
986 *Systems*, 10(7), 1571-1586. <https://doi.org/10.1029/2017MS001231>
- 987 Xin, X., Wu, T., Zhang, J., Yao, J., & Fang, Y. (2020). Comparison of CMIP6 and



- 988 CMIP5 simulations of precipitation in China and the East Asian summer monsoon.
989 International Journal of Climatology, 40(15), 6423-6440.
990 <https://doi.org/10.1002/joc.6590>
- 991 Xu, W., Liu, L., Cheng, M., Zhao, Y., Zhang, L., Pan, Y., Zhang, X., Gu, B., Li, Y.,
992 Zhang, X., Shen, J., Lu, L., Luo, X., Zhao, Y., Feng, Z., Collett Jr, J. L., Zhang,
993 F., & Liu, X. (2018). Spatial-temporal patterns of inorganic nitrogen air
994 concentrations and deposition in eastern China. Atmospheric Chemistry and
995 Physics, 18(5), 10931–10954. <https://doi.org/10.5194/acp-18-10931-2018>
- 996 Xu, W., Luo, X., Pan, Y., Zhang, L., Tang, A., Shen . J., Zhang, Y., Li, H., Wu, Q.,
997 Yang, D., Zhang, Y., Xue, J., Li, W., Li, Q., Tang, L., Lu, S., Liang, T., Tong, Y.,
998 Liu, P., Zhang, Q., Xiong, Z., Shi, X., Wu, L., Shi, W., Tian, K., Zhong, X., Shi,
999 K., Tang, Q., Zhang, L., Huang, J., He, C., Kuang, F., Zhu, B., Liu, H., Jin, X.,
1000 Xin, Y., Shi, X., Du, E., Dore, A., Tang, S., Collett Jr, J., Goulding, K., Sun, Y.,
1001 Ren, J., Zhang, F., & Liu, X. (2015) Quantifying atmospheric nitrogen deposition
1002 through a nationwide monitoring network across China. Atmospheric Chemistry
1003 and Physics, 15(21), 12345–12360. <https://doi.org/10.5194/acp-15-12345-2015>
- 1004 Xu, W., Zhang, L., & Liu, X. (2019). A database of atmospheric nitrogen concentration
1005 and deposition from the nationwide monitoring network in China. Scientific Data,
1006 6(1), 51. <https://doi.org/10.1038/s41597-019-0061-2>
- 1007 Xu, Z., Han, Y., Tam, C. Y., Yang, Z. L., & Fu, C. (2021). Bias-corrected CMIP6 global
1008 dataset for dynamical downscaling of the historical and future climate (1979–
1009 2100). Scientific Data, 8(1), 293. <https://doi.org/10.1038/s41597-021-01079-3>
- 1010 Yu, G., Jia, Y., He, N., Zhu, J., Chen, Z., Wang, Q., Piao, S., Liu, X., He, H., Guo, X.,
1011 Wen, Z., Li, P., Ding, G., & Goulding, K. (2019). Stabilization of atmospheric
1012 nitrogen deposition in China over the past decade. Nature Geoscience, 12(6), 424–
1013 429. <https://doi.org/10.1038/s41561-019-0352-4>
- 1014 Zhai, S., Jacob, D. J., Wang, X., Liu, Z., Wen, T., Shah, V., Li, K., Moch, J. M., Bates,
1015 K. H., Song, S., Shen, L., Zhang, Y., Luo, G., Yu, F., Sun, Y., Wang, L., Qi, M.,
1016 Tao, J., Gui, K., Xu, H., Zhang, Q., Zhao, T., Wang, Y., Lee, H. C., Choi, H., &



- 1017 Liao, H. (2021). Control of particulate nitrate air pollution in China. *Nature*
1018 *Geoscience*, 14, 389-395. <https://doi.org/10.1038/s41561-021-00726-z>
- 1019 Zhang, J., Gao, Y., Leung, L. R., Luo, K., Liu, H., Lamarque, J. -F., Fan J., Yao, X.,
1020 Gao, H., & Nagashima, T. (2019). Impacts of climate change and emissions on
1021 atmospheric oxidized nitrogen deposition over East Asia. *Atmospheric Chemistry*
1022 *and Physics*, 19(2), 887-900. <https://doi.org/10.5194/acp-19-887-2019>
- 1023 Zhang, L., Chen, Y., Zhao, Y., Henze, D. K., Zhu, L., Song, Y., Paulot, F., Liu, X., Pan,
1024 Y., Lin, Y., & Huang, B. (2018). Agricultural ammonia emissions in China:
1025 reconciling bottom-up and top-down estimates. *Atmospheric Chemistry and*
1026 *Physics*, 18(1), 339–355. <https://doi.org/10.5194/acp-18-339-2018>
- 1027 Zhang, Y., Foley, K. M., Schwede, D. B., Bash, J. O., Pinto, J. P., & Dennis, R. L. (2019).
1028 A Measurement-Model Fusion Approach for Improved Wet Deposition Maps and
1029 Trends. *Journal of Geophysical Research: Atmospheres*, 124(7), 4237-4251.
1030 <https://doi.org/10.1029/2018JD029051>
- 1031 Zhao, B., Wang, S. X., Liu, H., Xu, J. Y., Fu, K., Klimont, Z., Hao, J. M., He, K. B.,
1032 Cofala, J., & Amann, M. (2013). NO_x emissions in China: historical trends and
1033 future perspectives. *Atmospheric Chemistry and Physics*, 13(19), 9869–9897.
1034 <https://doi.org/10.5194/acp-13-9869-2013>
- 1035 Zhao, Y., Xi, M., Zhang, Q., Dong, Z., Ma, M., Zhou, K., Xu, W., Xing, J., Zheng, B.,
1036 Wen, Z., Liu, X., Nielsen, C. P., Liu, Y., Pan, Y., & Zhang, L. (2022). Decline in
1037 bulk deposition of air pollutants in China lags behind reductions in emissions.
1038 *Nature Geoscience*, 15(3), 190–195. <https://doi.org/10.1038/s41561-022-00899-1>
- 1039 Zhao, Y, Zhang, L., Chen, Y., Liu, X., Xu, W., Pan, Y., & Duan, L. (2017).
1040 Atmospheric nitrogen deposition to China: A model analysis on nitrogen budget
1041 and critical load exceedance. *Atmospheric Environment*, 153, 32–40.
1042 <https://doi.org/10.1016/j.atmosenv.2017.01.018>
- 1043 Zheng, B., Tong, D., Li, M., Liu, F., Hong, C., Geng, G., Li, H., Li, X., Peng, L., Qi, J.,
1044 Yan, L., Zhang, Y., Zhao, H., Zheng, Y., He, K., & Zhang, Q. (2018). Trends in
1045 China’s anthropogenic emissions since 2010 as the consequence of clean air



- 1046 actions. *Atmospheric Chemistry and Physics*, 18(19), 14095–14111.
1047 <https://doi.org/10.5194/acp-18-14095-2018>
- 1048 Zheng, L., Zhai, W., Wang, L., & Huang, T. (2020). Improving the understanding of
1049 central Bohai Sea eutrophication based on wintertime dissolved inorganic nutrient
1050 budgets: Roles of north Yellow Sea water intrusion and atmospheric nitrogen
1051 deposition. *Environmental Pollution*, 267, 115626.
1052 <https://doi.org/10.1016/j.envpol.2020.115626>
- 1053 Zhou, K., Xu, W., Zhang, L., Ma, M., Liu, X., & Zhao, Y. (2023). Estimating nitrogen
1054 and sulfur deposition across China during 2005 to 2020 based on multiple
1055 statistical models. *Atmospheric Chemistry and Physics*, 23(15), 8531-8551.
1056 <https://doi.org/10.5194/acp-23-8531-2023>
- 1057 Zhu, H., Chen, Y., Zhao, Y., Zhang, L., Zhang, X., Zheng, B., Liu, L., Pan Y., Xu, W.,
1058 & Liu, X. (2022). The Response of Nitrogen Deposition in China to Recent and
1059 Future Changes in Anthropogenic Emissions. *Journal of Geophysical Research:*
1060 *Atmospheres*, 127(23), e2022JD037437. <https://doi.org/10.1029/2022JD037437>
- 1061 Zhu, J., Chen, Z., Wang, Q., Xu, L., He, N., Jia, Y., Zhang, Q & Yu, G. (2020). Potential
1062 transition in the effects of atmospheric nitrogen deposition in China.
1063 *Environmental Pollution*, 258, 113739.
1064 <https://doi.org/10.1016/j.envpol.2019.113739>
- 1065 Zhu, J., Tai, A P K., & Hung Lam Yim, S. (2022). Effects of ozone–vegetation
1066 interactions on meteorology and air quality in China using a two-way coupled
1067 land–atmosphere model. *Atmospheric Chemistry and Physics*, 22(2), 765-782.
1068 <https://doi.org/10.5194/acp-22-765-2022>
1069



1070 **Figure captions**

1071 Figure 1 Evaluations of simulated monthly average temperature at the height of 2 m
1072 (T2, a), wind speed at the height of 10 m (WS10, b), relative humidity (RH, c), and
1073 accumulated precipitation (PREC, d) in Mainland China. The dots represent the site-
1074 level observations. The normalized mean bias (NMB), normalized mean error (NME),
1075 root mean squared error (RMSE) and the correlation coefficient (R) for the comparisons
1076 are shown in the lower left corner of each panel.

1077 Figure 2 Spatial distribution of annual averaged Nr deposition fluxes ($\text{kg N ha}^{-1} \text{ yr}^{-1}$)
1078 for different forms and species in 2010s and the changes between 2010s and 2060s.
1079 Panels (a-d) represent the results of 2010s (Base simulation). Panels (e-h) represent
1080 future deposition changes under the SSP2-4.5 pathway (Case 1 – Base). Panels (i-l)
1081 represent the changes under the SSP5-8.5 pathway (Case 2 – Base).

1082 Figure 3 Changes in annual total Nr deposition fluxes ($\text{kg N ha}^{-1} \text{ yr}^{-1}$) from 2010s to
1083 2060s attributed to climate change (a, d), emission change (b, e), and both (c, f). Panels
1084 (a-c) represent the changes under the SSP2-4.5 pathway, respectively and Panels (d-f)
1085 represent the changes under the SSP5-8.5 pathway. Domain-averaged spatial
1086 correlation (R) between the impact of climate or emission change and both is presented
1087 in panels (a, d) or (b, e).

1088 Figure 4 Changes in OXN (a-c) and RDN deposition (d-f) from 2010s to 2060s
1089 attributed to emission variation in “Baseline”, “Current-goal” and “Neutral-goal”
1090 scenarios.

1091 Figure 5 Relative changes in Nr emissions and deposition in WC and EC from 2010s
1092 to 2060s under different emission scenarios.

1093 Figure 6 Predicted response (%) of OXN (a-d) and RDN deposition (e-h) to a 20%
1094 perturbation of emissions in 2010s and 2060s for different emission scenarios. The
1095 response is obtained by calculating the ratio of the percent change in deposition to that
1096 in emission.



1097 **Tables**

1098 **Table 1 Description of the designed simulation cases.**

| Name | Emissions input | Meteorological input |
|--------|---|----------------------------|
| Base | MEIC, 2010-2014 | ERA5 reanalysis, 2010-2014 |
| Case1 | DPEC “Current-goal”, 2060 | SSP2-4.5 BCMM, 2060-2064 |
| Case2 | DPEC “Baseline”, 2060 | SSP5-8.5 BCMM, 2060-2064 |
| Case3 | MEIC, 2010-2014 | SSP2-4.5 BCMM, 2060-2064 |
| Case4 | MEIC, 2010-2014 | SSP5-8.5 BCMM, 2060-2064 |
| Case5 | DPEC “Neutral-goal”, 2060 | SSP2-4.5 BCMM, 2060-2064 |
| Case6 | Same as Case1, but emissions in WC are maintained at 2010s levels. | SSP2-4.5 BCMM, 2060-2064 |
| Case7 | Same as Case2, but emissions in WC are maintained at 2010s levels. | SSP5-8.5 BCMM, 2060-2064 |
| Case8 | Same as Case5, but emissions in WC are maintained at 2010s levels. | SSP2-4.5 BCMM, 2060-2064 |
| Case9 | Same as Case3, but with 20% reduction in emissions for all species. | SSP2-4.5 BCMM, 2060-2064 |
| Case10 | Same as Case1, but with 20% reduction in emissions for all species. | SSP2-4.5 BCMM, 2060-2064 |
| Case11 | Same as Case2, but with 20% reduction in emissions for all species. | SSP5-8.5 BCMM, 2060-2064 |
| Case12 | Same as Case5, but with 20% reduction in emissions for all species. | SSP2-4.5 BCMM, 2060-2064 |

1099

1100



1101

1102 **Table 2 The normalized mean bias (NMB), normalized mean error (NME) and the**
1103 **correlation coefficient (R) between the simulated and observed annual Nr**
1104 **deposition. Dry and wet Nr deposition fluxes of oxidized nitrogen (OXN) and**
1105 **reduced nitrogen (RDN) averaged over 2010-2014 were evaluated separately.**

| | OXN_DDEP | OXN_WDEP | RDN_DDEP | RDN_WDEP |
|-------------|----------|----------|----------|----------|
| NMB (%) | -9.07 | -15.12 | -28.76 | -17.86 |
| NME (%) | 34.76 | 43.24 | 47.17 | 41.72 |
| R(temporal) | 0.63 | 0.65 | 0.65 | 0.82 |
| R(spatial) | 0.73 | 0.72 | 0.83 | 0.69 |

1106 Note: OXN_DDEP and OXN_WDEP indicate the dry and wet deposition of oxidized nitrogen,
1107 respectively. RDN_DDEP and RDN_WDEP indicate the dry and wet deposition of reduced nitrogen,
1108 respectively.
1109



1110 **Table 3 Simulated atmospheric Nr deposition fluxes ($\text{kg N ha}^{-1} \text{ yr}^{-1}$) in China**
1111 **averaged over 2010-2014 and 2060-2064 under different SSP-RCP pathways.**

| Periods | Species | Dry | Wet | Total |
|---|-----------|-----|-----|-------|
| 2010-2014 (Case 1) | OXN | 3.7 | 3.4 | 7.1 |
| | RDN | 3.0 | 4.6 | 7.6 |
| | OXN + RDN | 6.7 | 8.0 | 14.7 |
| 2060-2064 under SSP2-4.5 (Case 2) | OXN | 1.5 | 1.6 | 3.1 |
| | RDN | 2.9 | 3.0 | 5.9 |
| | OXN + RDN | 4.4 | 4.6 | 9.0 |
| 2060-2064 under SSP5-8.5 (Case 3) | OXN | 4.0 | 4.4 | 8.4 |
| | RDN | 2.9 | 4.1 | 7.0 |
| | OXN + RDN | 6.9 | 8.5 | 15.4 |

1112



1113

1114 **Table 4 Simulated domain-averaged OXN deposition fluxes ($\text{kg N ha}^{-1} \text{ yr}^{-1}$) over**
1115 **EC for cases where emissions change to 2060s levels in all regions as well as cases**
1116 **where emissions in WC are maintained at 2010s levels. Relative changes (%) are**
1117 **calculated by comparing cases with 2060s emission levels in all regions to cases**
1118 **with 2010s emission levels in WC, then dividing the difference by the 2010s**
1119 **emission levels in WC.**

| | Emissions in WC are maintained at 2010s levels | Emissions change to 2060s levels in all regions | Relative change |
|----------------|---|--|--------------------|
| “Baseline” | 13.29 (Case7) | 13.59 (Case2) | 2% |
| “Current-goal” | 5.36 (Case6) | 5.08 (Case1) | -6% |
| “Neutral-goal” | 1.90 (Case8) | 1.39 (Case5) | -27% |

1120

1121



1122

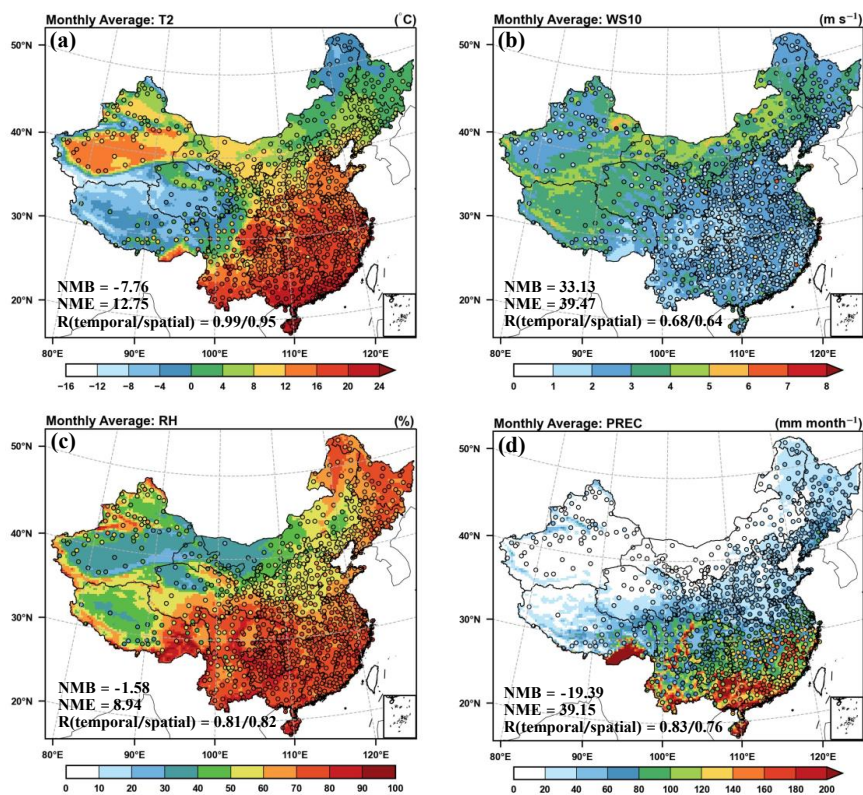
1123 **Table 5 Regional average responses (%) of OXN or RDN deposition to a 20%**
1124 **emission reduction in 2010s and 2060s under different emission scenarios over NC**
1125 **and SC and the whole of mainland China.**

| | NC | SC | China |
|--|--------|--------|-------|
| Responses (%) of OXN deposition to NO_x emissions | | | |
| 2010s | 82.60 | 96.19 | 82.71 |
| 2060s under “Baseline” | 83.95 | 92.54 | 88.41 |
| 2060s under “Current-goal” | 91.86 | 103.00 | 81.17 |
| 2060s under “Neutral-goal” | 94.59 | 98.07 | 68.83 |
| Responses (%) of RDN deposition to NH₃ emissions | | | |
| 2010s | 103.11 | 97.63 | 96.30 |
| 2060s under “Baseline” | 104.67 | 98.42 | 98.05 |
| 2060s under “Current-goal” | 100.70 | 95.99 | 94.38 |
| 2060s under “Neutral-goal” | 97.12 | 95.47 | 92.44 |

1126



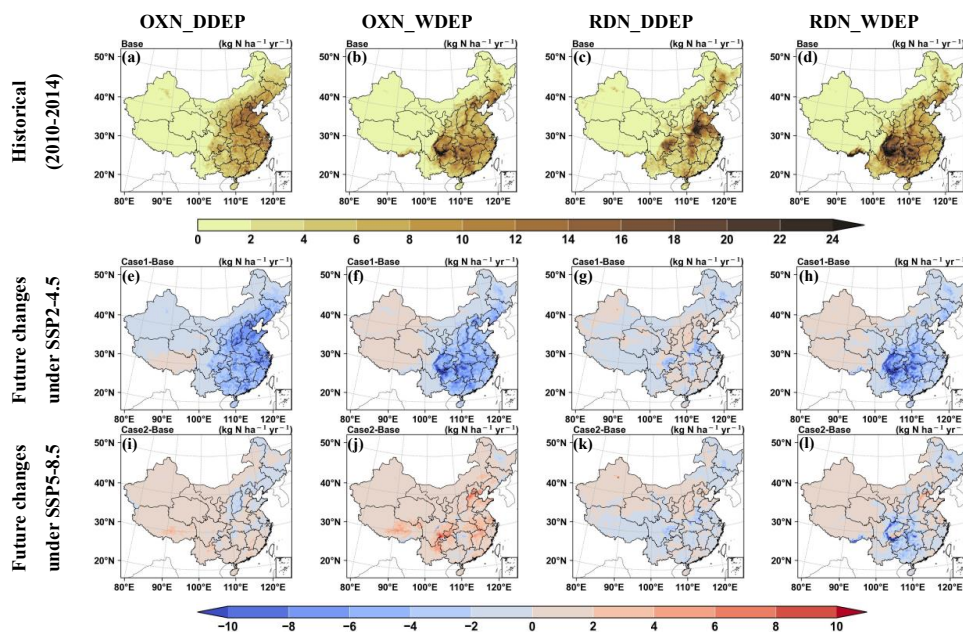
1127 **Figure 1**



1128



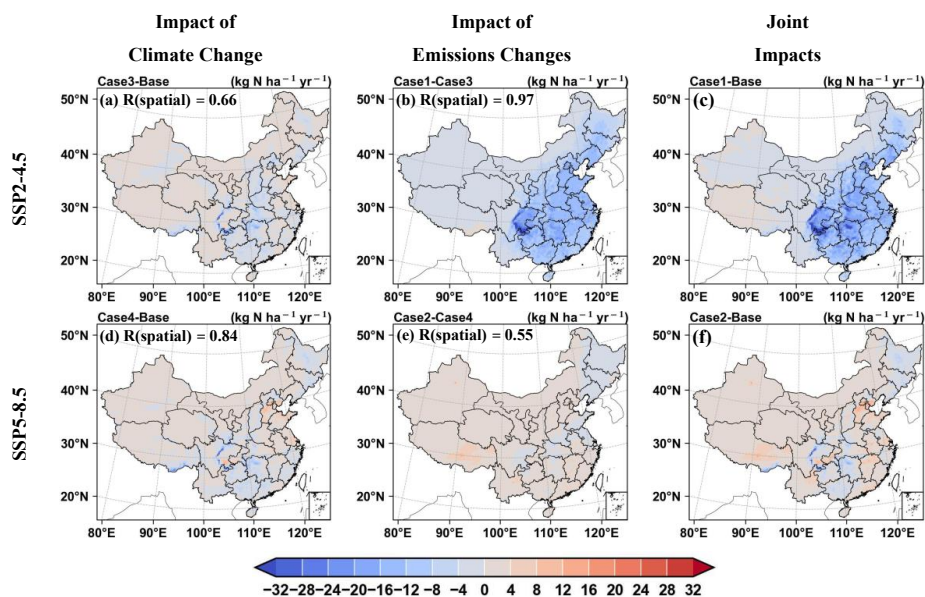
1129 **Figure 2**



1130



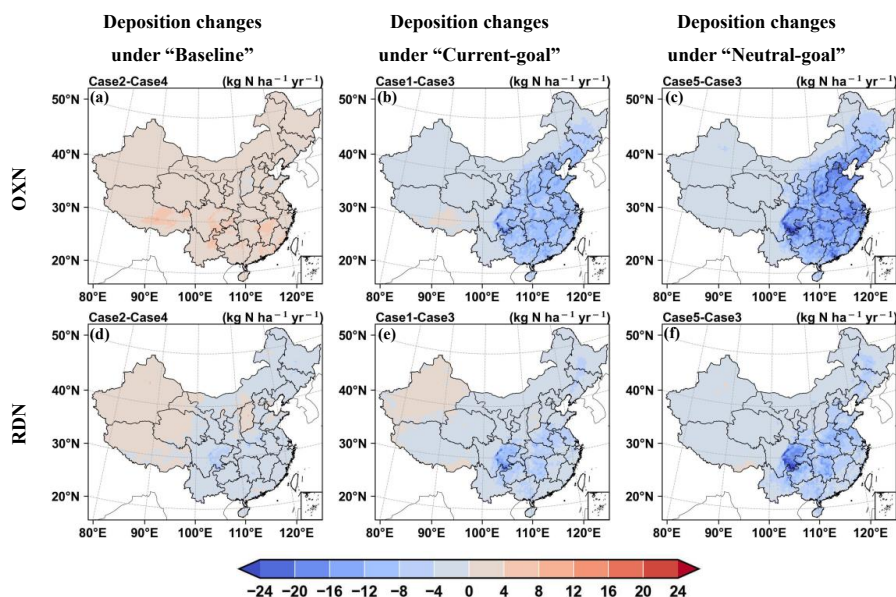
1131 **Figure 3**



1132



1133 **Figure 4**



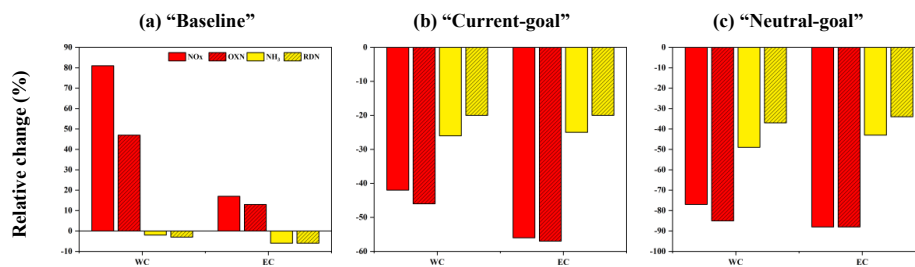
1134



1135

1136 **Figure 5**

1137



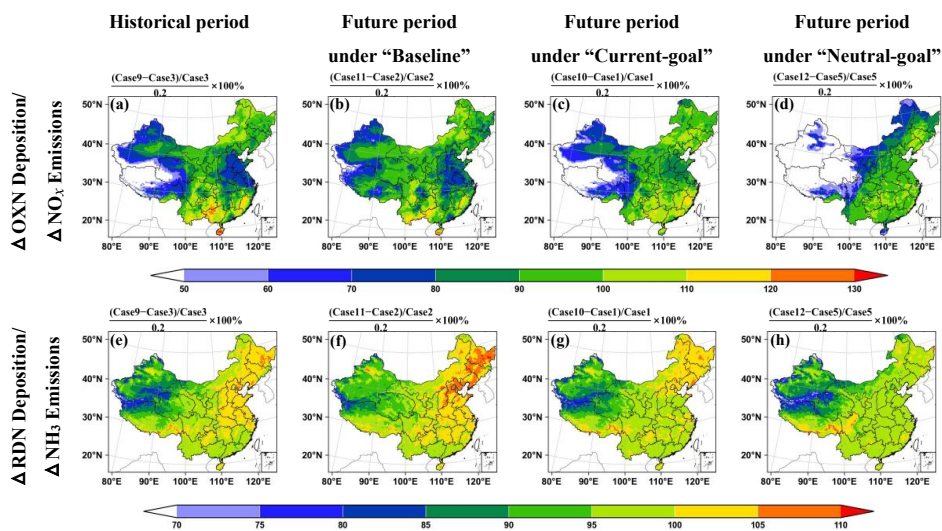
1138

1139



1140 **Figure 6**

1141



1142